

UNCLASSIFIED

AD NUMBER

AD047597

LIMITATION CHANGES

TO:

Approved for public release; distribution is unlimited.

FROM:

Distribution authorized to U.S. Gov't. agencies and their contractors;
Administrative/Operational Use; JUN 1954. Other requests shall be referred to Air Force Cambridge Research Laboratory, Hanscom AFB, MA.

AUTHORITY

usafgl ltr 2 nov 1981

THIS PAGE IS UNCLASSIFIED

THIS REPORT HAS BEEN DELIMITED
AND CLEARED FOR PUBLIC RELEASE
UNDER DOD DIRECTIVE 5200.20 AND
NO RESTRICTIONS ARE IMPOSED UPON
ITS USE AND DISCLOSURE.

DISTRIBUTION STATEMENT A

APPROVED FOR PUBLIC RELEASE,
DISTRIBUTION UNLIMITED.

Services Technical Information Agency

Due to our limited supply, you are requested to return this copy WHEN IT HAS SERVED PURPOSE so that it may be made available to other requesters. Your cooperation is appreciated.

47597

WHEN GOVERNMENT OR OTHER DRAWINGS, SPECIFICATIONS OR OTHER DATA IS FOR ANY PURPOSE OTHER THAN IN CONNECTION WITH A DEFINITELY RELATED GOVERNMENT PROCUREMENT OPERATION, THE U. S. GOVERNMENT THEREBY INCURS NO LIABILITY, NOR ANY OBLIGATION WHATSOEVER, AND THE FACT THAT THE GOVERNMENT MAY HAVE FORMULATED, FURNISHED, OR IN ANY WAY SUPPLIED THE DRAWINGS, SPECIFICATIONS, OR OTHER DATA IS NOT TO BE REGARDED BY ANY PERSON OR OTHERWISE AS IN ANY MANNER LICENSING THE HOLDER OR ANY OTHER PERSON OR CORPORATION, OR CONVEYING ANY RIGHTS OR PERMISSION TO MANUFACTURE, OR TO USE, ANY PATENTED INVENTION THAT MAY IN ANY WAY BE RELATED THERETO.

Reproduced by
DOCUMENT SERVICE CENTER
KNOTT BUILDING, DAYTON, 2, OHIO

DECLASSIFIED

4759
XEROGRAPHIC COPY
AFCRC.TN 54-175

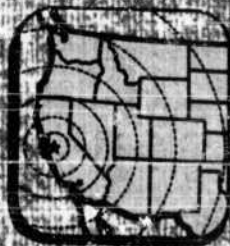
TECHNICAL REPORT 45

RADIATION FROM CURRENT ELEMENTS
AND APERTURES IN THE PRESENCE
OF A PERFECTLY CONDUCTING
HALF-PLANE SHEET

by

C. T. Tai

Air Force Contract No. AF 19 (604)-266



STANFORD RESEARCH INSTITUTE

Applied Research Center of the West

STANFORD, CALIFORNIA

STANFORD RESEARCH INSTITUTE

STANFORD, CALIFORNIA

JUNE 1954

TECHNICAL REPORT 45 - SRI PROJECT 591

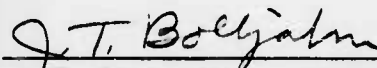
RADIATION FROM CURRENT ELEMENTS AND APERTURES IN THE PRESENCE OF A PERFECTLY CONDUCTING HALF-PLANE SHEET

by

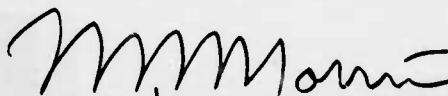
C. T. TAI

AIR FORCE CONTRACT NO. AF 19(604)-266

APPROVED:



J. T. BOLLJAHN
Head, Radio Systems Laboratory



T. H. MORRIN
Director of Engineering Research

COPY NO. 100

ABSTRACT

The application of the dyadic Green's function technique to a number of electromagnetic problems involving a perfectly conducting half-plane sheet is discussed. A derivation of the dyadic Green's function is given by the method of Fourier and Hankel transforms. Several sets of curves have been presented to show the radiation patterns in the principal plane for different excitations. The radiation resistance of a quarter-wave monopole attached to the edge of a half-plane sheet, and that of a half-wave dipole placed parallel to the edge of the sheet are also evaluated.

CONTENTS

ABSTRACT	ii
LIST OF ILLUSTRATIONS	iv
I INTRODUCTION	1
II DYADIC GREEN'S FUNCTION PERTAINING TO A PERFECTLY CONDUCTING HALF-PLANE SHEET	2
III APPLICATION FOR THE DYADIC GREEN'S FUNCTIONS TO RADIATION FROM DIPOLES AND APERTURES IN THE PRESENCE OF A HALF-PLANE SHEET	9
A. RADIATION FROM ELECTRIC DIPOLES	9
1. Longitudinal Electric Dipoles	9
2. Horizontal Electric Dipole	11
3. Vertical Electric Dipole	12
B. RADIATION FROM MAGNETIC DIPOLES	12
1. Longitudinal Magnetic Dipole	12
2. Horizontal Magnetic Dipole	12
3. Vertical Magnetic Dipole	12
C. RADIATION FROM APERTURES	13
1. Longitudinal Slot	13
2. Horizontal Slot	13
IV LOCATIONS OF THE MAXIMA AND MINIMA OF THE RADIATION PATTERN FOR SOURCES FAR AWAY FROM THE EDGE	16
V RADIATION RESISTANCE OF ANTENNAS NEAR HALF-PLANE SHEETS, AND RADIATION CONDUCTANCE OF THE COMPLEMENTARY SLOTS	18
A. QUARTER-WAVE MONOPOLE ATTACHED TO THE EDGE OF A HALF-PLANE SHEET	18
B. HALF-WAVE DIPOLE PLACED PARALLEL TO THE EDGE OF A HALF-PLANE SHEET	20
ACKNOWLEDGEMENT	23
REFERENCES	24
APPENDIX	25
TECHNICAL REPORTS IN THIS SERIES	54

ILLUSTRATIONS

	PAGE
Fig. 1 Half Plane Sheet	27
Figs. 2A-2F Radiation Pattern of a Longitudinal Dipole Placed in Front of a Half-Plane Sheet	28-33
Figs. 3A-3F Radiation Pattern of a Horizontal Dipole Placed in Front of a Half-Plane Sheet	34-39
Figs. 4A-4C Radiation Pattern of a Vertical Dipole Placed in Front of a Half-Plane Sheet	40-42
Fig. 5 Radiation Pattern of a One Sided Longitudinal Slot	43
Fig. 6 Radiation Pattern of a Two Sided Longitudinal Slot	44
Fig. 7 Radiation Pattern of a Small One-Sided Horizontal Aperture	45
Fig. 8 Radiation Pattern of a Small Two-Sided Horizontal Aperture	46
Fig. 9 Radiation Pattern of a Longitudinal Slot Placed at $ka = 30$	47
Fig. 10 Roots of the Equation $\frac{0.5 + C(x)}{0.5 + S(x)} = -\tan x$	48
Fig. 11 Dipoles and Slots with a Half-Plane Sheet	49
Fig. 12 The Functions $\left(\frac{n}{2}\right)^2 I_{\frac{n}{2}}^2(\theta) \frac{1}{\sin \theta}$ and $K_{\frac{n}{2}}^2(\theta) \cos^2 \theta \sin \theta$	50
Fig. 13 Input Impedance of a Stub Placed at the Edge of a Half-Plane Sheet	51
Fig. 14 Radiation Resistance of a Half-Wave Dipole Placed in Front of a Half-Plane Sheet, and in Front of a Ground Plane	52
Fig. 15 Radiation Resistance of a Half-Wave Dipole Placed near a Wedge, $R_d = \alpha (kd)^{2\mu_1}$ in Ohms	53

RADIATION FROM CURRENT ELEMENTS AND APERTURES IN THE PRESENCE OF A PERFECTLY CONDUCTING HALF-PLANE SHEET

I INTRODUCTION

Among the boundary-value problems involving a perfectly conducting half-plane sheet, the problem of diffraction of a plane polarized wave was treated long ago by Sommerfeld¹ by applying the theory of multi-valued functions of a complex variable to the formulation of the problem. The same problem can also be formulated and solved by using the Hopf-Wiener integral equation technique.^{2 3} In this report, problems involving dipoles and apertures as exciting sources will be discussed. By applying the technique of dyadic Green's functions, the electromagnetic field due to electric and magnetic dipoles in the presence of a half-plane sheet and the related problems involving apertures can be formulated in a compact manner. For certain ranges of the parameters, corresponding to the far-zone region, the complex integral that represents the formal solution can be evaluated approximately by means of the saddle-point method of integration to yield some pertinent information regarding the radiation pattern in the principal plane. The radiation field can, of course, be obtained by applying the reciprocal theorem and making use of Sommerfeld's solution. The method adopted here, however, seems to be more direct. As a whole, the general formulation not only gives a better view of the relationship between various problems but also provides a foundation for further investigation in subjects not covered in this work, particularly the near-zone field.

II DYADIC GREEN'S FUNCTION PERTAINING TO A PERFECTLY CONDUCTING HALF-PLANE SHEET

It is well known in electromagnetic theory that for a harmonic varying field with a time dependence of the form $e^{-i\omega t}$, the electric and the magnetic vectors satisfy the following two equations:

$$\nabla \times \nabla \times \mathbf{E} - k^2 \mathbf{E} = i\omega\mu \mathbf{J}_e \quad (1)$$

$$\nabla \times \nabla \times \mathbf{H} - k^2 \mathbf{H} = \nabla \times \mathbf{J}_e \quad (2)$$

where \mathbf{J}_e denotes the electric current density function. In dealing with radiation from circulating currents it is convenient to introduce an equivalent magnetic current density function \mathbf{J}_m defined by

$$\nabla \times \mathbf{J}_e = i\omega\epsilon \mathbf{J}_m \quad (3)$$

Equation (2) can then be written in a form similar to Eq. (1)

$$\nabla \times \nabla \times \mathbf{H} - k^2 \mathbf{H} = i\omega\epsilon \mathbf{J}_m \quad (4)$$

To integrate Eqs. (1) and (4) two dyadic Green's functions, denoted respectively by $\underline{\mathbf{G}}_e$ and $\underline{\mathbf{G}}_m$, are introduced. They both satisfy the equation

$$\nabla \times \nabla \times \underline{\mathbf{G}} - k^2 \underline{\mathbf{G}} = \underline{\mathbf{I}} \delta(x - x') \delta(y - y') \delta(z - z') \quad (5)^*$$

where $\underline{\mathbf{I}}$ denotes the unit dyadic or idem factor. The electric dyadic Green's function satisfies the boundary condition that at the surface of a perfectly conducting body

$$\mathbf{n} \times \underline{\mathbf{G}}_e = 0 \quad (6)$$

* In regard to notations used in this paper, the bold face type is used for vectors; boldface type with a bar denotes a dyadic.

while the magnetic dyadic Green's function is characterized by

$$\mathbf{n} \times \nabla \times \underline{\mathbf{G}}_{\mathbf{n}} = 0. \quad (7)$$

Once the explicit expressions of $\underline{\mathbf{G}}_{\mathbf{e}}$ and $\underline{\mathbf{G}}_{\mathbf{n}}$ are known, the formal solution for the electromagnetic field due to a given source in the presence of a perfectly conducting body can be presented in the form of certain integrals. If the exciting source consists of current elements, the electric field is given by

$$\mathbf{E} = i\omega\mu \iiint \mathbf{J}'_{\mathbf{e}} \cdot \underline{\mathbf{G}}_{\mathbf{e}} dv' \quad (8)$$

If the source is made of apertures on the conducting body with a given electric field distribution, then

$$\mathbf{E} = \iint_{\text{apertures}} (\mathbf{E}' \times \mathbf{n}') \cdot \nabla' \times \underline{\mathbf{G}}_{\mathbf{e}} dS' \quad (9)$$

For the case of circulating currents as exciting sources, the magnetic field is given by

$$\mathbf{H} = i\omega\epsilon \iiint \mathbf{J}'_{\mathbf{n}} \cdot \underline{\mathbf{G}}_{\mathbf{n}} dv' \quad (10)$$

The corresponding electric field is

$$\mathbf{E} = - \iiint \nabla \times [\mathbf{J}'_{\mathbf{n}} \cdot \underline{\mathbf{G}}_{\mathbf{n}}] dv' \quad (11)$$

Equations (8) - (11) constitute the basic formulae to be used in studying the radiation from current elements and apertures in the presence of a perfectly conducting body.

Let us now consider a perfectly conducting half-plane sheet as the diffracting body. The half-plane is defined by $y = 0$ and $x \geq 0$ in the Cartesian coordinate system (Fig. 1). The longitudinal axis of the half-plane is parallel to the z -axis. For convenience, the entire x - y plane corresponding to $z = 0$ will be designated as the principal plane. The method used here to derive the dyadic Green's functions pertaining to this structure follows very closely the one described by Morse and Feshbach⁴ in dealing with the interior boundary value problems of a circular cylinder. The main difference is that the spectrum of eigenvalues in the present

problem is continuous both in the z -coordinate and the r -coordinate, where r is the cylindrical radial coordinate defined in the x - y plane.

Like all other cylindrical problems the elementary vector wave functions that are needed to construct \underline{G} are of two kinds defined as follows:

$$\underline{M} = \nabla \times (\psi \underline{z}) \quad (12)$$

$$\underline{N} = k_c^{-1} \nabla \times \underline{M} = k_c^{-1} \nabla \times \nabla \times (\psi \underline{z}) \quad (13)$$

where ψ denotes an eigen function satisfying the scalar wave equation

$$\nabla^2 \psi + k_c^2 \psi = 0. \quad (14)$$

The wave number k_c is, at this point, completely arbitrary. The appropriate scalar eigen functions that will satisfy the boundary conditions on a half-plane sheet are

$$\psi_{o(n/2)\lambda_c}^{(ih)} = e^{ihz} J_{\frac{n}{2}}(\lambda_c r) \frac{\cos\left(\frac{n\phi}{2}\right)}{\sin\left(\frac{n\phi}{2}\right)} \quad (15)$$

with

$$\lambda_c^2 = k_c^2 - h^2, \quad n = 0, 1, \dots$$

In Eq. (15), $J_{\frac{n}{2}}(\lambda_c r)$ denotes the Bessel Function of order $n/2$, and (r, ϕ, z) are the circular cylindrical coordinates. The corresponding vector wave functions are then given by

$$\underline{M}_{o(n/2)\lambda_c}^{(ih)} = e^{ihz} \underline{m}_{o(n/2)\lambda_c}^{(ih)} \quad (16a)$$

$$\underline{m}_{o(n/2)\lambda_c}^{(ih)} = \left[\mp \frac{n}{2r} J_{\frac{n}{2}}(\lambda_c r) \frac{\sin\left(\frac{n\phi}{2}\right)}{\cos\left(\frac{n\phi}{2}\right)} \underline{r} - \lambda_c J_{\frac{n}{2}}'(\lambda_c r) \frac{\cos\left(\frac{n\phi}{2}\right)}{\sin\left(\frac{n\phi}{2}\right)} \underline{\phi} \right] \quad (16b)$$

$$\underline{N}_{o(n/2)\lambda_c}^{(ih)} = e^{ihz} \underline{n}_{o(n/2)\lambda_c}^{(ih)} \quad (17a)$$

$$\underline{n}_{o(n/2)\lambda_c}^{(ih)} = \left[\frac{ih\lambda_c}{k_c} J_{\frac{n}{2}}'(\lambda_c r) \frac{\cos\left(\frac{n\phi}{2}\right)}{\sin\left(\frac{n\phi}{2}\right)} \underline{r} \mp \frac{ihn}{k_c r} J_{\frac{n}{2}}(\lambda_c r) \frac{\sin\left(\frac{n\phi}{2}\right)}{\cos\left(\frac{n\phi}{2}\right)} \underline{\phi} + \frac{\lambda_c^2}{k_c} J_{\frac{n}{2}}(\lambda_c r) \frac{\cos\left(\frac{n\phi}{2}\right)}{\sin\left(\frac{n\phi}{2}\right)} \underline{z} \right] \quad (17b)$$

Since the derivations of \underline{G}_e and \underline{G}_o are very similar, only the former will be considered in detail. To express \underline{G}_e in terms of these vector wave functions, one needs only the M_e and N_o functions because they are the only functions that would satisfy the boundary condition stated by Eq. (6). In order to solve Eq. (5), using the method of orthogonal functions, the orthogonal property of the two sets of vector wave functions must first be established.

Consider two arbitrary sets of eigenvalues denoted, respectively, by $(n/2, \lambda_c, h)$ and $(n'/2, \lambda'_c, h')$. It can easily be shown that

$$\left. \begin{aligned} \int_0^{2\pi} m_{e(n/2)\lambda_c} \cdot m_{e(n'/2)\lambda'_c} d\phi &= 0, \\ \int_0^{2\pi} n_{o(n/2)\lambda_c} \cdot n_{o(n'/2)\lambda'_c} d\phi &= 0, \\ \int_0^{2\pi} n_{o(n/2)\lambda_c} \cdot m_{e(n'/2)\lambda'_c} d\phi &= 0. \end{aligned} \right\} n \neq n' \quad (18)$$

By applying the formula of Hankel that

$$\int_0^\infty \lambda_c d\lambda_c \int_0^\infty r dr J_\mu(\lambda'_c r) J_\mu(\lambda_c r) f(\lambda_c) = f(\lambda'_c) \quad (19)$$

one finds that for $n = n'$

$$\int_0^\infty \lambda_c d\lambda_c \int_0^\infty r dr \int_0^{2\pi} d\phi \left\{ \begin{aligned} &m_{e(n/2)\lambda_c} \cdot m_{e(n/2)\lambda'_c} \\ &n_{o(n/2)\lambda_c} \cdot n_{o(n/2)\lambda'_c}(-ih) \end{aligned} \right\} = (1 + \delta_0) \pi \lambda_c'^2 \quad (20)$$

while

$$\int_0^\infty \lambda_c d\lambda_c \int_0^\infty r dr \int_0^{2\pi} d\phi m_{o(n/2)\lambda_c} \cdot m_{e(n/2)\lambda'_c} = 0. \quad (21)$$

In Eq. (20) $n_{o(n/2)\lambda'_c}(-ih)$ denotes the function $n_{o(n/2)\lambda'_c}$ with the sign of ih reversed. It may be remarked here that the normalization regarding these vector wave functions for the case in which the n 's are even integers has been discussed by Stratton.⁵ The orthogonal relationship between $m_{o(n/2)\lambda_c}$ and $m_{e(n'/2)\lambda'_c}$, however, was not correctly established. The two functions are, in general, not orthogonal with respect to ϕ , although they

are orthogonal in the entire domain of r , λ_c , and ϕ . To derive the explicit expression for \underline{G} , let us first expand the right side of Eq. (5) in terms of $M_{e(n/2)\lambda_c}(ih)$ and $N_{o(n/2)\lambda_c}(ih)$ as follows:

$$\underline{I} \delta(x - x') \delta(y - y') \delta(z - z') =$$

$$\int_0^\infty \lambda_c d\lambda_c \int_{-\infty}^\infty dh \sum_{n=0}^\infty \left[A_n(-ih) M_{e(n/2)\lambda_c}(ih) + B_n(-ih) N_{o(n/2)\lambda_c}(ih) \right] \quad (22)$$

where A_n and B_n are two unknown functions to be determined. The double integration contained in Eq. (22) indicates that the eigenvalues are continuous both in the r and the z coordinates. Taking the scalar product of Eq. (22) with $M'_{e(n'/2)\lambda'_c}(-ih')$ and $N'_{o(n'/2)\lambda'_c}(-ih')$, respectively, and then integrating with respect to dv over all space, one obtains

$$\left. \begin{aligned} M'_{e(n'/2)\lambda'_c}(-ih') \\ N'_{o(n'/2)\lambda'_c}(-ih') \end{aligned} \right\} = \int_0^\infty r dr \int_{-\infty}^\infty dz \int_0^{2\pi} d\phi \int_0^\infty \lambda_c d\lambda_c \int_{-\infty}^\infty dh \cdot$$

$$\cdot \sum_{n=0}^\infty \left[A_n(-ih) M_{e(n/2)\lambda_c}(ih) + B_n(-ih) N_{o(n/2)\lambda_c}(ih) \right] \cdot$$

$$\cdot \begin{cases} M_{e(n'/2)\lambda'_c}(-ih') \\ N_{o(n'/2)\lambda'_c}(-ih') \end{cases} \quad (23)$$

The prime functions at the left side of Eq. (23) are defined in the prime coordinates (r', ϕ', z') . The multiple integral contained in Eq. (23) can be simplified by making use of the orthogonal relations described by Eqs. (18) - (21), and the Fourier integral theorem

$$\int_{-\infty}^\infty dz \int_{-\infty}^\infty dh [e^{i(h-h')z} f(h)] = 2\pi f(h') \quad (24)$$

to obtain

$$M'_{e(n'/2)\lambda'_c}(-ih') = 2\pi^2 (1 + \delta_0) \lambda'_c{}^2 A_{n'}(-ih') \quad (25)$$

$$N'_{o(n'/2)\lambda'_c}(-ih') = 2\pi^2 (1 + \delta_0) \lambda'_c{}^2 B_{n'}(-ih') \quad (26)$$

hence,

$$\begin{aligned} \mathbb{I} \delta(x - x') \delta(y - y') \delta(z - z') &= \int_0^\infty d\lambda_c \int_{-\infty}^\infty dh \cdot \\ &\cdot \sum_{n=0} \frac{2 - \delta_0}{4\pi^2 \lambda_c} \left[M'_{e(n/2)\lambda_c}(-ih) M_{e(n/2)\lambda_c}(ih) \right. \\ &\quad \left. + N'_{o(n/2)\lambda_c}(-ih) N_{o(n/2)\lambda_c}(ih) \right] . \end{aligned} \quad (27)$$

To determine \underline{G}_e , one writes

$$\begin{aligned} \underline{G}_e &= \int_0^\infty d\lambda_c \int_{-\infty}^\infty dh \sum_{n=0} C_n \left[M'_{e(n/2)\lambda_c}(-ih) M_{e(n/2)\lambda_c}(ih) \right. \\ &\quad \left. + N'_{o(n/2)\lambda_c}(-ih) N_{o(n/2)\lambda_c}(ih) \right] , \end{aligned} \quad (28)$$

where C_n is an unknown function of λ_c and h . The unknown function can be determined by substituting Eqs. (27) and (28) into Eq. (5) to obtain

$$C_n = \frac{2 - \delta_0}{4\pi^2 \lambda_c (h^2 + \lambda_c^2 - k^2)} \quad (29)$$

and hence,

$$\begin{aligned} \underline{G}_e &= \int_0^\infty d\lambda \int_{-\infty}^\infty dh \sum_{n=0} \frac{(2 - \delta_0)}{4\pi^2 \lambda_c (h^2 + \lambda_c^2 - k^2)} \cdot \\ &\cdot \left[M'_{e(n/2)\lambda_c}(-ih) M_{e(n/2)\lambda_c}(ih) + N'_{o(n/2)\lambda_c}(-ih) N_{o(n/2)\lambda_c}(ih) \right] . \end{aligned} \quad (30)$$

The integration with respect to λ_c can be simplified by making use of the identity that

$$\int_0^\infty \frac{J_{\frac{n}{2}}(\lambda_c r') J_{\frac{n}{2}}(\lambda_c r) f(\lambda_c)}{\lambda^2 - \lambda_c^2} d\lambda_c = \frac{\pi}{2i\lambda} f(\lambda) \begin{cases} J_{\frac{n}{2}}(\lambda r') H_{\frac{n}{2}}^{(1)}(\lambda r), & r > r' \\ J_{\frac{n}{2}}(\lambda r) H_{\frac{n}{2}}^{(1)}(\lambda r'), & r < r' . \end{cases} \quad (31)$$

It is assumed that λ is the only pole of the integrand. The final expression of \underline{G}_e is therefore given by

$$\underline{G}_e = \frac{i}{8\pi} \int_{-\infty}^{\infty} dh \sum_{n=0}^{\infty} \frac{2 - \delta_0}{\lambda^2}.$$

$$\begin{cases} M'_{e(n/2)\lambda}(-ih) M^{(3)}_{e(n/2)\lambda}(ih) + N'_{e(n/2)\lambda}(-ih) N^{(3)}_{e(n/2)\lambda}(ih), & r > r' \quad (32a) \\ M'_{e(n/2)\lambda}(-ih) M^{(1)}_{e(n/2)\lambda}(ih) + N'_{e(n/2)\lambda}(-ih) N^{(1)}_{e(n/2)\lambda}(ih), & r < r' \quad (32b) \end{cases}$$

where

$$\lambda^2 = k^2 - h^2.$$

The superscripts (1) and (3) are the conventional notations for the two kinds of vector wave functions with different cylindrical functions. Thus,

$$M^{(1)}_{e(n/2)\lambda}(ih) = \nabla \times \left[e^{ihz} J_{\frac{n}{2}}(\lambda r) \cos\left(\frac{n\phi}{2}\right) z \right] \quad (33)$$

$$M^{(3)}_{e(n/2)\lambda}(ih) = \nabla \times \left[e^{ihz} H^{(1)}_{\frac{n}{2}}(\lambda r) \cos\left(\frac{n\phi}{2}\right) z \right] \quad (34)$$

and similarly for the N-functions.

In regard to the magnetic dyadic Green's function the deviation is practically the same. The only difference is that the vector functions M_e and N_e are now used to construct \underline{G}_n so that the boundary condition stated by Eq. (7) is satisfied. The final expression for \underline{G}_n is therefore similar to that of \underline{G}_e , except that M_e and N_e in \underline{G}_e are replaced by M_n and N_n for \underline{G}_n . Because of the mutual relationship that

$$\nabla \times M_{e(n/2)\lambda} = k N_{e(n/2)\lambda} \quad (35)$$

$$\nabla \times N_{e(n/2)\lambda} = k M_{e(n/2)\lambda} \quad (36)$$

it is obvious that

$$\nabla \times \nabla' \times \underline{G}_e = k^2 \underline{G}_e \quad (37)$$

and

$$\nabla \times \nabla' \times \underline{G}_n = k^2 \underline{G}_n \quad (38)$$

With slight modifications the method described here can be used to derive the dyadic Green's functions pertaining to other cylindrical structures.

III APPLICATION FOR THE DYADIC GREEN'S FUNCTIONS TO RADIATION FROM DIPOLES AND APERTURES IN THE PRESENCE OF A HALF-PLANE SHEET

Once the expressions for \underline{G}_e and \underline{G}_m are known the discussion of the radiation from given current elements or apertures with given field distribution reduces to that of evaluating some complex integrals. In general, integrals of the type contained in Eqs. (8)-(11) are difficult to evaluate. However, for certain restricted ranges of the parameters, corresponding to the far-zone region, most of the integrals can be evaluated in a closed form. Depending upon the nature of the exciting sources, the problems can most conveniently be divided into three groups:

- Radiation from Electric Dipoles
- Radiation from Magnetic Dipoles
- Radiation from Slots Cut in the Half-Plane Sheet

A. RADIATION FROM ELECTRIC DIPOLES

1. LONGITUDINAL ELECTRIC DIPOLE

Let us first consider an electric dipole with moment p_z , oriented along the direction of the longitudinal axis of the half-plane sheet. The dipole is placed at $(a, \varphi_0, 0)$. The electric current density function can be written as

$$\underline{J}_e = -i\omega p_z \delta(r - a) \delta(\varphi - \varphi_0) \delta(z - 0) \hat{\underline{z}} \quad (39)$$

Substituting Eqs. (32a) and (39) into Eq. (8), one finds that the longitudinal component of the electric field is given by

$$E_z = \frac{ip_z}{4\pi\epsilon} \int_{-\infty}^{\infty} \lambda^2 e^{i\lambda z} \sum_{n=1}^{\infty} \sin\left(\frac{n\varphi_0}{2}\right) \sin\left(\frac{n\varphi}{2}\right) J_{\frac{n}{2}}(\lambda a) H_{\frac{n}{2}}^{(1)}(\lambda r) d\lambda \quad (40)$$

For large values of kR , where R , θ , and φ are the spherical coordinates of the point of observation, the complex integral continued in Eq. (40)

can be evaluated approximately by means of the saddle-point method of integration, with the result

$$E_z = \frac{\omega^2 \mu \rho_z}{2\pi} \frac{e^{i k R}}{R} \sin^2 \theta \sum_{n=1}^{\infty} (-1)^{\frac{n}{2}} \sin\left(\frac{n\varphi_0}{2}\right) \sin\left(\frac{n\varphi}{2}\right) J_{\frac{n}{2}}(ka \sin \theta) \quad (41)$$

Because of the reciprocal relationship between the properties of transmitting and receiving antennas it can be inferred from Sommerfeld's diffraction theory that one should be able to transform the series in Eq. (41) into certain Fresnel integrals which represent the original form of Sommerfeld's solution. The transformation can be done either by applying an expansion theorem due to Hargreaves⁶ in connection with the half-order Bessel functions or by using an alternative method described by Morse and Feshbach⁷. It has been shown by these authors that if one writes

$$S(\rho, \varphi) = \frac{1}{2} \sum_{n=0}^{\infty} (2 - \delta_0) \cos\left(\frac{n\varphi}{2}\right) J_{\frac{n}{2}}(\rho) \quad (42)$$

the integral representation of the series is given by

$$S(\rho, \varphi) = (\pi)^{-\frac{1}{2}} e^{-i(\rho \cos \varphi + \frac{\pi}{4})} \int_{-\infty}^{\sqrt{2\rho} \cos(\frac{\varphi}{2})} e^{i s^2} ds \quad (43)$$

The integral contained in Eq. (43) can be transformed into the standard Fresnel integrals defined as follows:

$$C(x) = \int_0^x \frac{\cos t}{(2\pi t)^{\frac{1}{2}}} dt, \quad S(x) = \int_0^x \frac{\sin t}{(2\pi t)^{\frac{1}{2}}} dt \quad (44)$$

Adequate tabulations are available for these two functions^{8,9}. For numerical computation the following formula for $S(\rho, \varphi)$ is therefore more desirable

$$S(\rho, \varphi) = 2^{-\frac{1}{2}} e^{-i(\rho \cos \varphi + \frac{\pi}{4})} \left\{ \frac{1}{2} (1 + i) \pm [C(x) + iS(x)] \right\}, \quad (45)$$

$$x = ka(1 + \cos \varphi)$$

where the sign is fixed according to the range of φ

$$\begin{cases} + & 0 \leq \varphi \leq \pi \\ - & \pi \leq \varphi \leq 2\pi \end{cases}$$

Regarding $S(\rho, \varphi)$ as an "elementary" function, one can reduce Eq. (41) into the following form

$$E_z = \frac{\omega^2 \mu \varphi_z e^{ikR}}{4\pi R} \sin^2 \theta [S(ka \sin \theta, \varphi - \varphi_0) - S(ka \sin \theta, \varphi + \varphi_0)] \quad (46)$$

In the principal plane, corresponding to $\theta = 90^\circ$, the radiation pattern of the z-component of the electric field due to a longitudinal electric dipole in the presence of the half-plane sheet is therefore simply given by

$$F(E_z) = S(ka, \varphi - \varphi_0) - S(ka, \varphi + \varphi_0) \quad (47)$$

It is, of course, possible to obtain the same information regarding the radiation pattern from Sommerfeld's solution by applying the reciprocal theorem. Equation (47) also contains the essential result obtained by Harrington,¹⁰ concerning the radiation pattern of a line source in the presence of a half-plane sheet. In fact the complex integral obtained by Harrington based upon the solution of the Hopf-Wiener integral equation can readily be reduced into Fresnel integrals.

For other orientations of the dipole, the derivation of the essential formulae concerning the radiation pattern in the principal plane is practically the same. The final results are summarized below.

2. HORIZONTAL ELECTRIC DIPOLE (IN THE DIRECTION OF x-AXIS)

$$\begin{aligned} F(E_\phi) = \sin \varphi [S(ka, \varphi - \varphi_0) - S(ka, \varphi + \varphi_0)] \\ + \left(\frac{2}{\pi ka}\right)^{\frac{1}{2}} e^{i(ka + \frac{\pi}{4})} \sin\left(\frac{\varphi_0}{2}\right) \cos\left(\frac{\varphi}{2}\right) \end{aligned} \quad (48)$$

3. VERTICAL ELECTRIC DIPOLE (IN THE DIRECTION OF Y-AXIS)

$$F(E_\phi) = \cos \phi [S(ka, \phi - \phi_0) + S(ka, \phi + \phi_0)] + \left(\frac{2}{\pi ka}\right)^{\frac{1}{2}} e^{i(ka + \frac{\pi}{4})} \cos\left(\frac{\phi_0}{2}\right) \cos\left(\frac{\phi}{2}\right) \quad (49)$$

The patterns based upon Eqs. (47), (48), and (49), after being properly normalized, are plotted in Figs. 2, 3, and 4 for several different values of ka and ϕ_0 .

B. RADIATION FROM MAGNETIC DIPOLES

1. LONGITUDINAL MAGNETIC DIPOLE (IN THE DIRECTION OF Z-AXIS)

$$F(E_\phi) = S(ka, \phi - \phi_0) + S(ka, \phi + \phi_0) \quad (50)$$

2. HORIZONTAL MAGNETIC DIPOLE (IN THE DIRECTION OF X-AXIS)

$$F(E_z) = \sin \phi [S(ka, \phi - \phi_0) + S(ka, \phi + \phi_0)] + \left(\frac{2}{\pi ka}\right)^{\frac{1}{2}} e^{i(ka + \frac{\pi}{4})} \cos\left(\frac{\phi_0}{2}\right) \sin\left(\frac{\phi}{2}\right) \quad (51)$$

3. VERTICAL MAGNETIC DIPOLE (IN THE DIRECTION OF Y-AXIS)

$$F(E_z) = \cos \phi [S(ka, \phi - \phi_0) - S(ka, \phi + \phi_0)] - \left(\frac{2}{\pi ka}\right)^{\frac{1}{2}} e^{i(ka + \frac{\pi}{4})} \sin\left(\frac{\phi_0}{2}\right) \sin\left(\frac{\phi}{2}\right) \quad (52)$$

As shown in the following section, when a longitudinal magnetic dipole or a horizontal magnetic dipole is placed at the half-plane sheet, the pattern is the same as that of a small longitudinal slot or a small horizontal slot cut in the sheet.

C. RADIATION FROM APERTURES

The electromagnetic field due to apertures with given electric field distribution can be evaluated by applying Eq. (9). The aperture can be excited either "one-sided" or "two-sided." In practice, the one-sided excitation corresponds to the aperture radiation from a waveguide terminated by a half-plane sheet. If the opening on the sheet is fed by a two-wire transmission line or a coaxial transmission line the excitation would be two-sided. Much useful information regarding the radiation field due to apertures can be gathered by considering the radiation from narrow slots.

1. LONGITUDINAL SLOT

The field distribution for a narrow longitudinal slot can be written as

$$\mathbf{E} = f(z) \delta(r - a) \hat{\mathbf{r}} \quad (53)$$

where $f(z)$ is a given function of z depending upon the assumed field distribution along the slot. For a one-sided excitation the far-zone field in the principal plane, obtained by substituting Eqs. (32a) and (53) into Eq. (9) and applying the saddle-point method of integration, is

$$F_1(E_\phi) = S(ka, \phi) \quad (54)$$

The pattern is the same as that of a longitudinal magnetic dipole when the latter is placed at the surface of the half-plane sheet corresponding to $\phi_0 = 0$ and at a distance $r = a$ from the edge. The corresponding formula for a two-sided excitation is

$$\begin{aligned} F_2(E_\phi) &= S(ka, \phi) - S(ka, 2\pi - \phi) \\ &= \pm (2)^{\frac{1}{2}} e^{-i(ka \cos \phi + \frac{\pi}{4})} [C(x) + iS(x)] , \\ x &= ka(1 + \cos \phi) \end{aligned} \quad (55)$$

2. HORIZONTAL SLOT

The radiation field due to a horizontal slot is somewhat more difficult to evaluate. Assuming that the field distribution in the slot is of the form

$$E = f(r) \delta(z - 0) \hat{z}, \quad (56)$$

where $f(r)$ is a given function of r , then the far-zone field in the principal plane due to a one-sided slot is, in general, given by

$$E_z = \frac{e^{ikR}}{4\pi R} \sum_{n=1}^{\infty} n(-i)^{\frac{n}{2}} \sin\left(\frac{n\varphi}{2}\right) \int_{\text{slot}} \frac{f(r') J_{\frac{n}{2}}(kr')}{r'} dr'. \quad (57)$$

The integral contained in Eq. (57) cannot be evaluated in closed form unless the function $f(r')$ is a delta function so that the analysis applies to the problem of a very short slot or one of another class of functions discussed in a later section. As present, let us consider the special case of a short slot. Replacing $f(r')$ in Eq. (57) by $\delta(r'-a)$, where a is the radial distance measured from the edge of the half-plane sheet to the small opening, one obtains

$$\begin{aligned} E_z &= \frac{e^{ikR}}{4\pi aR} \sum_{n=1}^{\infty} n(-i)^{\frac{n}{2}} J_{\frac{n}{2}}(ka) \sin\left(\frac{n\varphi}{2}\right) \\ &= -\frac{e^{ikR}}{4\pi aR} \frac{\partial}{\partial \varphi} S(ka, \varphi) \end{aligned} \quad (58)$$

The radiation pattern of a one-sided small horizontal slot in the principal plane is therefore given by

$$\begin{aligned} F_1(E_z) &= \frac{1}{ika} \frac{\partial}{\partial \varphi} S(ka, \varphi) \\ &= \sin \varphi S(ka, \varphi) + \frac{e^{i(ka + \frac{\pi}{4})}}{(2\pi ka)^{\frac{1}{2}}} \sin\left(\frac{\varphi}{2}\right). \end{aligned} \quad (59)$$

The pattern is, of course, the same as that of a horizontal magnetic dipole placed at the surface of the sheet obtained by putting $\varphi_0 = 0$ in Eq. (51). The corresponding formula for a two-sided small horizontal slot is

$$\begin{aligned}
 F_2(E_z) = & |\sin \varphi| e^{-ikac \cos \phi} [C(x) + i S(x)]_{x=ka(1+\cos \phi)} \\
 & + \frac{ie^{ika}}{(nka)^{\frac{1}{2}}} \sin\left(\frac{\varphi}{2}\right)
 \end{aligned} \tag{60}$$

Patterns based upon Eqs. (54), (55), and (60) are plotted in Figs. 5-8 for several different values of ka .

IV LOCATIONS OF THE MAXIMA AND MINIMA OF THE RADIATION PATTERN FOR SOURCES FAR AWAY FROM THE EDGE

Since extensive tables of the Fresnel Integrals are available, it is possible to compute the radiation patterns corresponding to various excitations for practically any value of ka . If the value of ka is large, the pattern exhibits certain distinct properties. A typical pattern for a one-sided longitudinal slot placed a distance corresponding to $ka = 30$ from the edge of the sheet is shown in Fig. 9. The locations of the maxima and the minima of such a pattern can be ascertained in a relatively simple manner. In the case of a one-sided longitudinal slot, the extreme values of the pattern are determined by the condition

$$\frac{\partial |S(ka, \varphi)|}{\partial \varphi} = 0 \quad (61)$$

Using the explicit expression of $S(ka, \varphi)$ given by Eq. (45), one obtains

$$\frac{\frac{1}{2} + C(x)}{\frac{1}{2} + S(x)} = -\tan x \quad (62)$$

where

$$x = ka(1 + \cos \varphi)$$

The graphical solution for the roots of Eq. (62) is shown in Fig. 10. Denoting these roots by x_n , one can see from Fig. 10 that the approximate solutions for the roots are given by

$$x_n = (4n - 1) \frac{\pi}{4} ,$$

or

$$\cos \varphi_n = (4n - 1) \frac{\pi}{4ka} - 1, \quad n = 1, 2, \dots \quad (63)$$

Equation (63) determines the locations of the maxima when m 's are odd integers. Interlaced between the maxima are the minima corresponding to even integers of m . Since the magnitude of $S(ka, \phi_1)$ and that of $S(ka, \pi)$ are independent of ka , their ratio

$$\frac{S(ka, \phi_1)}{S(ka, \pi)} = 0.428 \quad (64)$$

is therefore also independent of ka . It is a measure of the rapidity of the decay of the field from the peak value to the value observed at the boundary between the shadow region and the illuminated region. Similar discussions can be carried out for the fields set up by the other types of antennas considered above.

V RADIATION RESISTANCE OF ANTENNAS NEAR HALF-PLANE SHEETS, AND RADIATION CONDUCTANCE OF THE COMPLEMENTARY SLOTS

In this section we will discuss the radiation resistance of a quarter-wave monopole attached to the edge of a half plane sheet, and that of a half-wave dipole placed in front of the sheet with its axis parallel to the edge of the sheet as shown in Fig. 11 (a) and (b). The complementary problems of a quarter-wave slot normal to the edge of the sheet, and a half-wave slot cut in the sheet parallel to the edge, are shown in Fig. 11 (c) and (d). Since the Babinet-Booker relationship regarding the radiation resistance of the dipole and the radiation conductance of the complementary slot applies, namely

$$\frac{R_d}{G_s} = \frac{\eta^2}{4} \quad (65)$$

where

$$\eta = 120\pi \text{ ohms,}$$

it is therefore sufficient for our purpose to present only the detailed analysis for the cases involving the monopole and the dipole.

A. QUARTER-WAVE MONOPOLE ATTACHED TO THE EDGE OF A HALF-PLANE SHEET

To evaluate the radiation resistance of the monopole for this case, the method of Poynting-energy theorem will be applied. For a base-driven monopole it will be assumed that the current distribution is sinusoidal. The current density function to be used in Eq. (8) can therefore be written in the form

$$\mathbf{J}_e = I_0 \cos kr \frac{\delta(z-0) \delta(\phi-\pi)}{r} \hat{\mathbf{r}} \quad (66)$$

Using the expression of \mathbf{G}_e given by Eq. (32a), and applying the method of saddle-point integration, one can obtain the explicit expression for the far-zone electric field. Expressed in spherical coordinates, it is

$$\mathbf{E} = E_{\theta} \hat{\theta} + E_{\phi} \hat{\phi} \quad (67)$$

$$E_{\theta} = -\frac{\eta I_0 e^{ikR}}{2\pi R} \sum_{n=1,3,\dots} (i)^{\frac{n}{2}-1} \sin\left(\frac{n\varphi}{2}\right) \cos \theta K_{\frac{n}{2}}(\theta) \quad (67a)$$

$$E_{\phi} = -\frac{\eta I_0 e^{ikR}}{2\pi R} \sum_{n=1,3,\dots} (i)^{\frac{n}{2}-1} \cos\left(\frac{n\varphi}{2}\right) \frac{1}{\sin \theta} \left(\frac{n}{2}\right) I_{\frac{n}{2}}(\theta) \quad (67b)$$

where

$$K_{\frac{n}{2}}(\theta) = k \int_0^{\frac{\lambda}{4}} J'_{\frac{n}{2}}(kr \sin \theta) \cos kr \, dr \quad (68)$$

$$I_{\frac{n}{2}}(\theta) = \int_0^{\frac{\lambda}{4}} J_{\frac{n}{2}}(kr \sin \theta) \cos kr \frac{dr}{r} \quad (69)$$

The functions $K_{\frac{n}{2}}(\theta)$ and $I_{\frac{n}{2}}(\theta)$ defined in Eqs. (68) and (69) can be evaluated in terms of the Fresnel integrals. They are tabulated in the Appendix for $n = 1$ and 3 . Using Eqs. (67a) and (67b), one finds that the radiation resistance of the quarter-wave monopole defined with respect to the base current I_0 is given by

$$\begin{aligned} R_{\text{rad}} &= \frac{2}{\eta I_0^2} \int_0^{2\pi} \int_0^{\frac{\pi}{2}} (E_{\theta}^2 + E_{\phi}^2) R^2 \sin \theta \, d\theta d\varphi \\ &= \frac{\eta}{2\pi} \sum_{n=1,3,\dots} \left[\left(\frac{n}{2}\right)^2 \int_0^{\frac{\pi}{2}} \frac{I_{\frac{n}{2}}^2(\theta)}{\sin \theta} d\theta + \int_0^{\frac{\pi}{2}} K_{\frac{n}{2}}^2(\theta) \cos^2 \theta \sin \theta \, d\theta \right] \quad (70) \end{aligned}$$

The integrals contained in Eq. (70) can only be evaluated numerically.

The integrands $\left(\frac{n}{2}\right)^2 \frac{I_{\frac{n}{2}}^2(\theta)}{\sin \theta}$ and $K_{\frac{n}{2}}^2(\theta) \cos^2 \theta \sin \theta$ are plotted in

Fig. 12 for $n = 1$ and 3. The contributions to R_{rad} by terms with $n = 5$ and higher are negligible. The sum of the four leading terms gives a value of R_{rad} equal to 86.3 ohms. It is interesting to observe that the value is greater than the free-space radiation resistance of a half-wave dipole, namely 73.13 ohms. For a quarter-wave monopole driven against a ground plane, the radiation resistance is, of course, only 36.56 ohms. The input impedance of a monopole driven against a large, but finite, half-plane sheet has been measured experimentally. The result is plotted in Fig. 13. The antenna is a quarter-wavelength long at a frequency of 700 Mc. The input resistance of the antenna at this frequency is around 92 ohms. It confirms the calculated value of R_{rad} within the experimental error.

B. HALF-WAVE DIPOLE PLACED PARALLEL TO THE EDGE OF A HALF-PLANE SHEET

As in the previous case, it is assumed that the current distribution on the dipole is sinusoidal. The current density function to be used in Eq. (8) is

$$J_z = I_0 \cos kz \frac{\delta(r-d) \delta(\phi-\pi)}{r} \hat{z} \quad (71)$$

The far-zone field in this case has only one component, i.e., E_{θ} . Following the same procedure as before, one obtains

$$E_{\theta} = \frac{-\eta I_0 e^{ikR}}{\pi R} \frac{\cos\left(\frac{\pi}{2} \cos \theta\right)}{\sin \theta} \sum_{n=1,3,\dots} (i)^{\frac{n}{2}} J_{\frac{n}{2}}(kd \sin \theta) \sin\left(\frac{n\phi}{2}\right). \quad (72)$$

The radiation resistance of the dipole can be evaluated according to the following formula

$$\begin{aligned} R_{\text{rad}} &= \frac{2}{\eta I_0^2} \int_0^{2\pi} \int_0^{\frac{\pi}{2}} E_{\theta}^2 R^2 \sin \theta \, d\theta \, d\phi \\ &= \frac{2\eta}{\pi} \sum_{n=1,3,\dots} \int_0^{\frac{\pi}{2}} \frac{\cos^2\left(\frac{\pi}{2} \cos \theta\right)}{\sin \theta} J_{\frac{n}{2}}^2(kd \sin \theta) \, d\theta. \end{aligned} \quad (73)$$

The integrals contained in Eq. (73) may be evaluated numerically with the aid of an adequate table of half-order Bessel functions. The result is plotted in Fig. 14. For comparison, the radiation resistance of a horizontal half-wave dipole placed above a ground plane is also plotted in the same figure. The two curves are seen to intersect at those points when d is a multiple of a quarter wavelength. It is believed that the identity of the two equations for radiation resistance could be demonstrated at these points without difficulty, but such a demonstration has not been carried out. Physically, however, it is difficult to explain why the two configurations yield the same radiation resistance, since the field distribution of the two structures are entirely different.

Our discussion on the radiation resistance of a half-wave dipole in the presence of a half-plane sheet supplements the earlier work by Kraus¹¹ on the radiation resistance of a dipole placed in a corner reflector. A half-plane sheet is structurally a limiting case of corner reflector when the angle of the reflector approaches 360 deg. Using the dyadic Green's function pertaining to a perfectly conducting wedge, one can, indeed, treat the same types of problems as have been discussed here for a half-plane sheet.

As a conclusion of this report we shall consider the problem of the radiation resistance of a half-wave dipole placed in front of a perfectly conducting wedge when the distance between the dipole and the edge of the wedge is small compared to a wavelength. By an analysis similar to that leading to Eq. (73), the general formula for the radiation resistance of the dipole in this case may be shown to be

$$R_d = \frac{4\eta}{2\pi - \varphi_0} \sum_{n=1,3,\dots} \int_0^{\frac{\pi}{2}} \frac{\cos^2\left(\frac{n}{2} \cos \theta\right)}{\sin \theta} J_{\mu_n}^2(kd \sin \theta) d\theta \quad (74)$$

where

$$\varphi_0 = \text{angle of the wedge}$$

$$\mu_n = \frac{n\pi}{2\pi - \varphi_0}, \quad n = 1, 3, \dots$$

Because of the lack of adequate tables of Bessel Functions of arbitrary fractional order, the integrals in Eq. (74) cannot easily be evaluated.

In the case

$$\left(\frac{kd}{2}\right)^2 \ll \frac{\Gamma(\mu_1 + 2)}{\Gamma(\mu_1 + 1)}$$

the significant part in Eq. (74) is contributed by the leading term of $J_{\mu_1}(kd \sin \theta)$, which is given by

$$J_{\mu_1}(kd \sin \theta) \approx \frac{1}{\Gamma(\mu_1 + 1)} \left(\frac{1}{2} kd \sin \theta\right)^{\mu_1} \quad (75)$$

The radiation resistance of the dipole under this condition can be computed from the following formula:

$$R_d = \alpha (kd)^{2\mu_1} \quad (76)$$

where

$$\alpha = \frac{480\mu_1}{2^{2\mu_1}\Gamma^2(\mu_1 + 1)} \int_0^{\frac{\pi}{2}} \cos^2\left(\frac{\pi}{2} \cos \theta\right) (\sin \theta)^{2\mu_1-1} d\theta$$

The index $2\mu_1$ and the constant α are plotted in Fig. 15, as a function of the wedge angle ϕ_0 . When $2\pi - \phi_0 = \frac{\pi}{m}$ with $m = 1, 2, \dots$ the wedge becomes a regular corner reflector such that the method of images can be applied to determine the radiation field, and hence the radiation resistance, of the dipole as discussed by Kraus.

ACKNOWLEDGEMENT

The author is indebted to Dr. John T. Bolljahn for many valuable discussions in the course of this study. Mr. Ivan J. Stampalia has kindly supplied the experimental data mentioned in this report. The assistance of Mrs. E A. Clarke with numerical calculations is gratefully acknowledged.

REFERENCES

1. A. Sommerfield, *Math. Ann.* 45, 263 (1894), 47, 317 (1896); see also B. B. Baker and E. T. Copson, *The Mathematical Theory of Huygen's Principal* (Oxford University Press, Oxford, 1950) Chap. IV.
2. E. T. Copson, *Quar. Jour. of Math., Oxford Series*, 17, 19, (1946).
3. S. N. Karp, "Communications on Pure and Appl. Math.," Vol. III, No. 4, p. 411 (1950).
4. P. M. Morse and H. Feshbach, *Methods of Theoretical Physics* (Technology Press, Massachusetts Institute of Technology, Cambridge, Massachusetts, 1946) Chap. IX.
5. J. A. Stratton, *Electromagnetic Theory*, pp. 397-399; McGraw-Hill Book Co. Inc., New York; 1941.
6. R. Hargreaves, *Phil. Mag.* 36, 191 (1928).
7. Morse and Feshbach, *op. cit.*, pp. 364-365.
8. G. N. Watson, *Theory of Bessel Functions*, Cambridge University Press, London, 1922.
9. Robert Turner and Anne F. Downey, A Tabulation of the Fresnel Integrals, Tech. Rep. No. 173, Cruft Laboratory, Harvard University, Cambridge, Mass.
10. R. F. Harrington, *Jour. of Appl. Physics*, 24, 547 (1953).
11. J. D. Kraus, *Antennas*, pp. 328-336; McGraw-Hill Book Co. Inc., New York; 1950.

APPENDIX

THE FUNCTIONS $K_{\frac{n}{2}}(\theta)$ AND $I_{\frac{n}{2}}(\theta)$

$$K_{\frac{1}{2}}(\theta) = \frac{1}{(\sin \theta)^{\frac{1}{2}}} \left\{ \frac{1}{(1 + \sin \theta)^{\frac{1}{2}}} \left[1 - \left(\frac{1 + \sin \theta}{\sin \theta} \right) \right] C(\rho_+) \right. \\ \left. + \frac{1}{(1 + \sin \theta)^{\frac{1}{2}}} \left[1 + \left(\frac{1 - \sin \theta}{\sin \theta} \right) \right] C(\rho_-) \right\} ,$$

$$K_{\frac{3}{2}}(\theta) = \frac{1}{(\sin \theta)^{\frac{1}{2}}} \left\{ \frac{-4 \sin \left(\frac{\pi}{2} \sin \theta \right)}{\pi \sin^2 \theta} \right. \\ + \frac{1}{(1 + \sin \theta)^{\frac{1}{2}}} \left[1 - 3 \left(\frac{1 + \sin \theta}{\sin \theta} \right) + 2 \left(\frac{1 + \sin \theta}{\sin \theta} \right)^2 \right] S(\rho_+) \\ \left. + \frac{1}{(1 - \sin \theta)^{\frac{1}{2}}} \left[-1 - 3 \left(\frac{1 - \sin \theta}{\sin \theta} \right) - 2 \left(\frac{1 - \sin \theta}{\sin \theta} \right)^2 \right] S(\rho_-) \right\} ,$$

$$I_{\frac{1}{2}}(\theta) = \frac{1}{(\sin \theta)^{\frac{1}{2}}} \left\{ 2(1 + \sin \theta)^{\frac{1}{2}} C(\rho_+) - 2(1 - \sin \theta)^{\frac{1}{2}} C(\rho_-) \right\} ,$$

$$I_{\frac{3}{2}}(\theta) = \frac{1}{(\sin \theta)^{\frac{1}{2}}} \left\{ \frac{8 \sin \left(\frac{\pi}{2} \sin \theta \right)}{3\pi \sin \theta} + 2(1 + \sin \theta)^{\frac{1}{2}} \left[1 - \frac{2}{3} \left(\frac{1 + \sin \theta}{\sin \theta} \right) \right] S(\rho_+) \right. \\ \left. + 2(1 - \sin \theta)^{\frac{1}{2}} \left[1 + \frac{2}{3} \left(\frac{1 - \sin \theta}{\sin \theta} \right) \right] S(\rho_-) \right\} ,$$

where $S(\rho)$ and $C(\rho)$ are the Fresnel sine- and cosine-integrals. The arguments ρ_+ and ρ_- are defined as follows:

$$\rho_+ = \frac{\pi}{2} (1 + \sin \theta)$$

$$\rho_- = \frac{\pi}{2} (1 - \sin \theta)$$

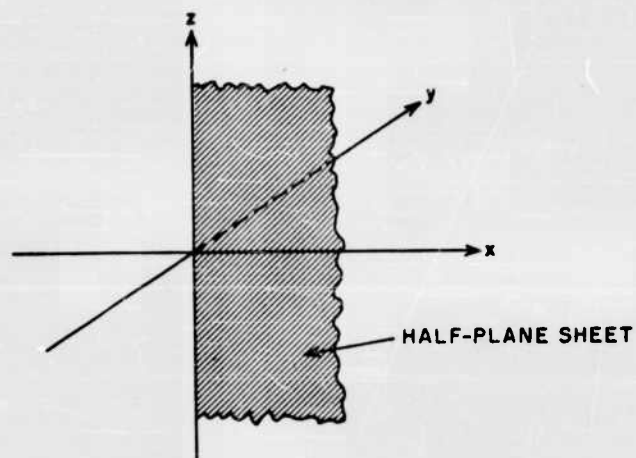


FIG. 1
HALF-PLANE SHEET

A-591-TR45-487

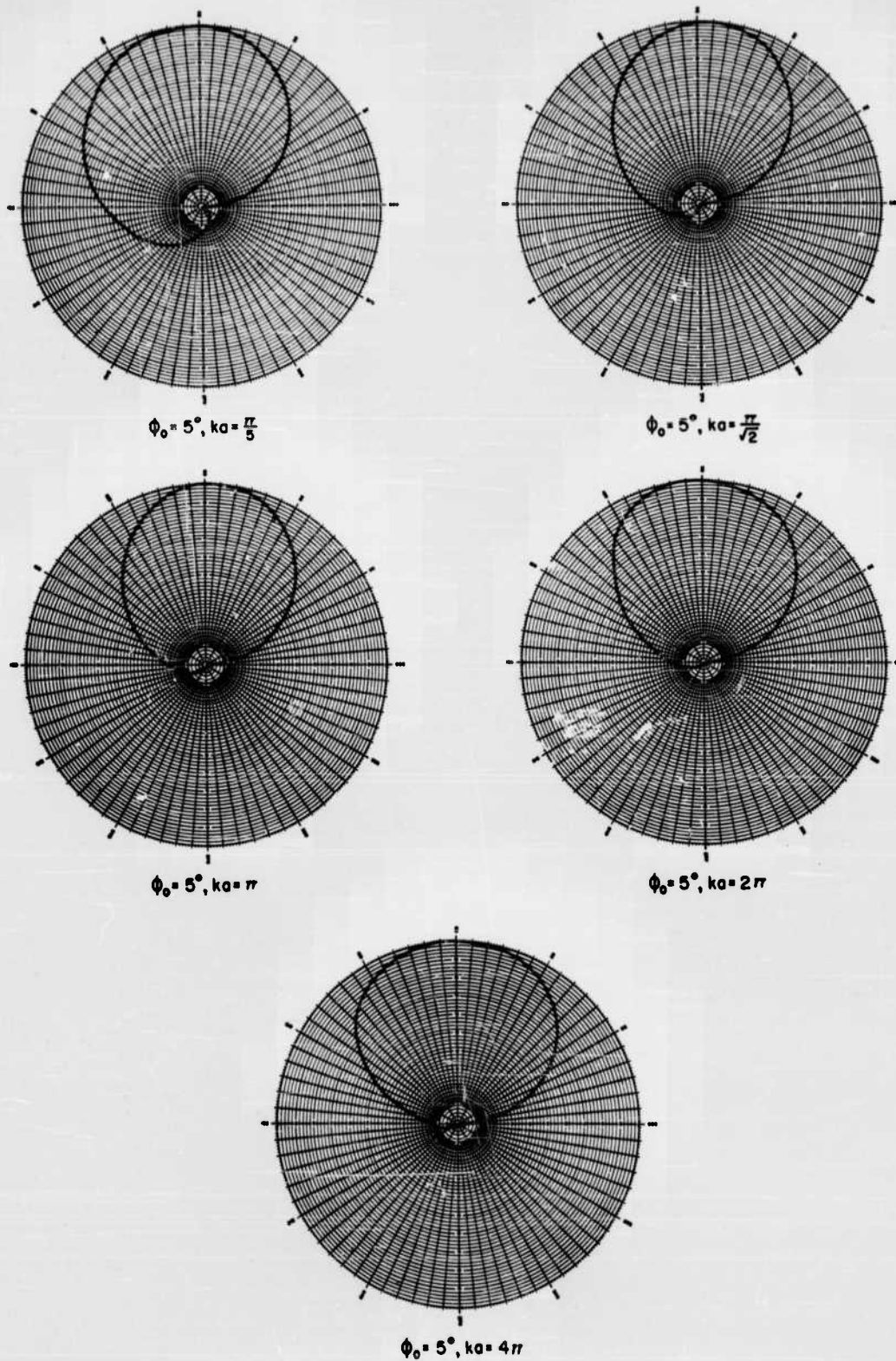
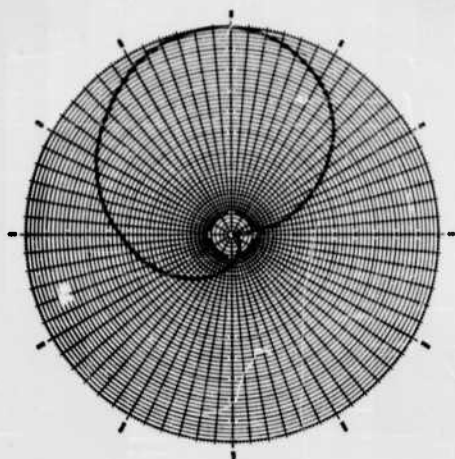
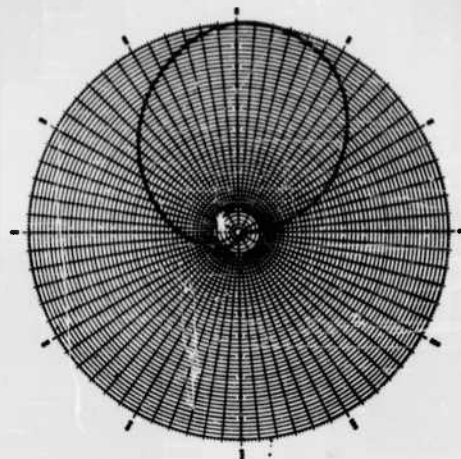


FIG. 2A
 RADIATION PATTERN OF A LONGITUDINAL DIPOLE
 PLACED IN FRONT OF A HALF-PLANE SHEET

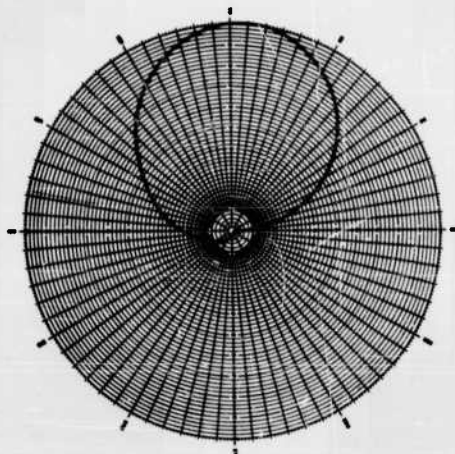
D-591-TR45-488



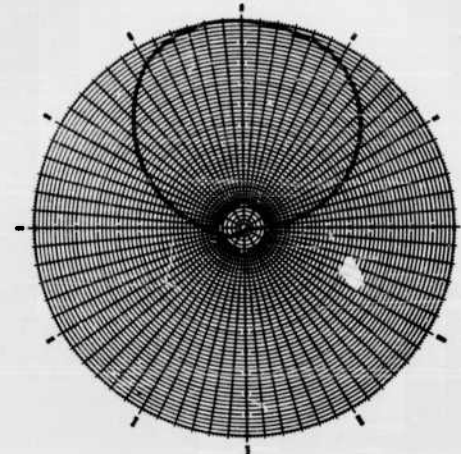
$$\phi_0 = 10^\circ, ka = \frac{\pi}{5}$$



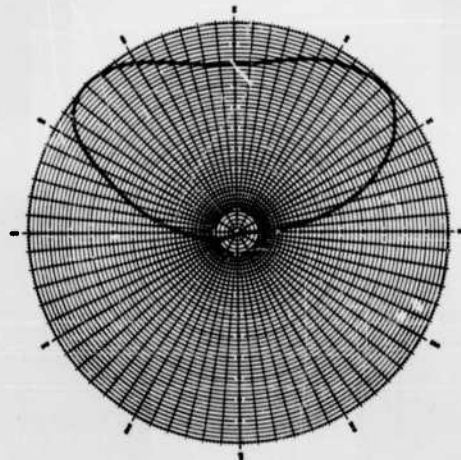
$$\phi_0 = 10^\circ, ka = \frac{\pi}{2}$$



$$\phi_0 = 10^\circ, ka = \pi$$



$$\phi_0 = 10^\circ, ka = 2\pi$$



$$\phi_0 = 10^\circ, ka = 4\pi$$

FIG. 2B

RADIATION PATTERN OF A LONGITUDINAL DIPOLE
PLACED IN FRONT OF A HALF-PLANE SHEET

D-591-TR45-489

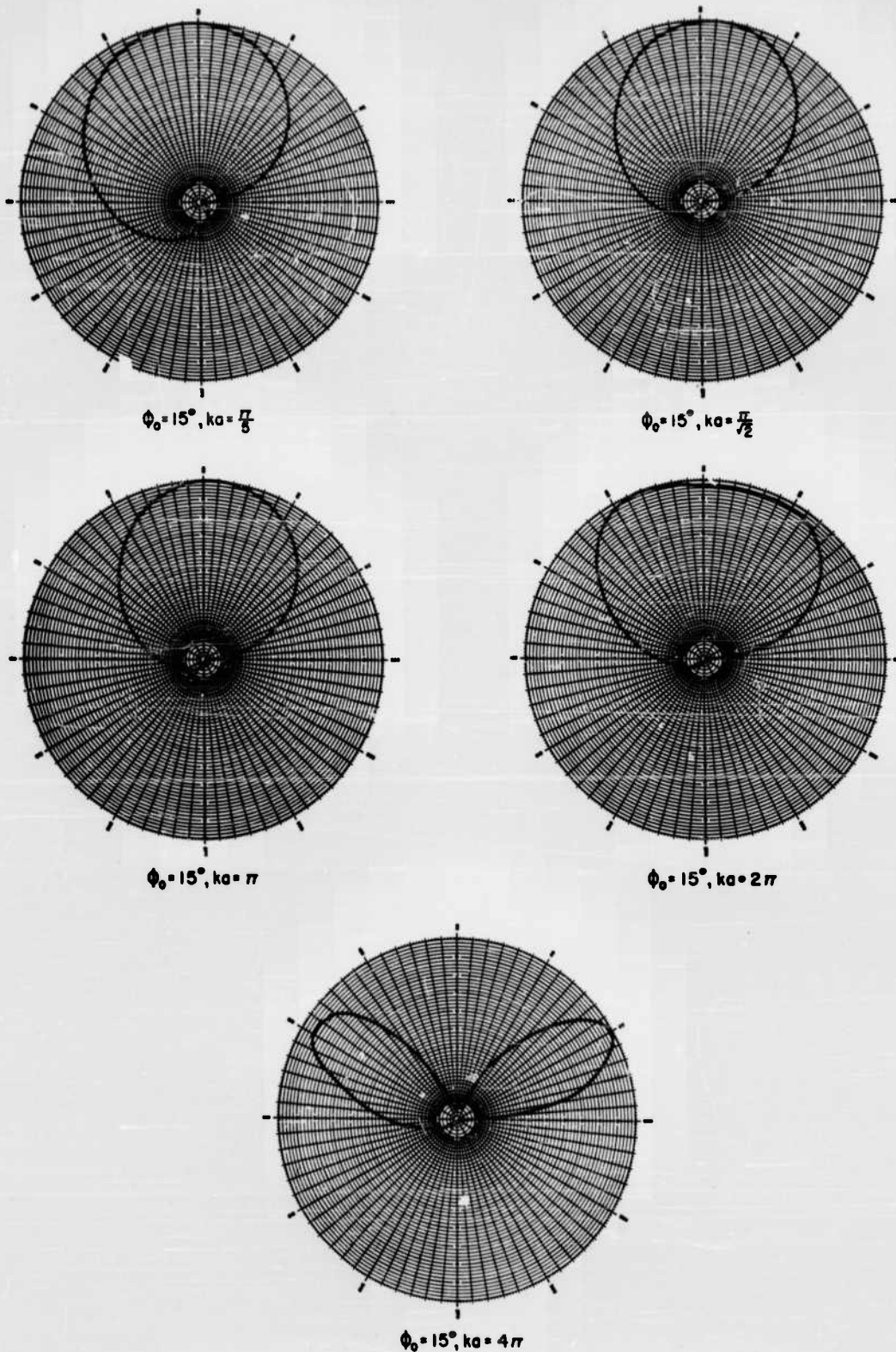


FIG. 2C
 RADIATION PATTERN OF A LONGITUDINAL DIPOLE
 PLACED IN FRONT OF A HALF-PLANE SHEET
 D-591-TR45-490

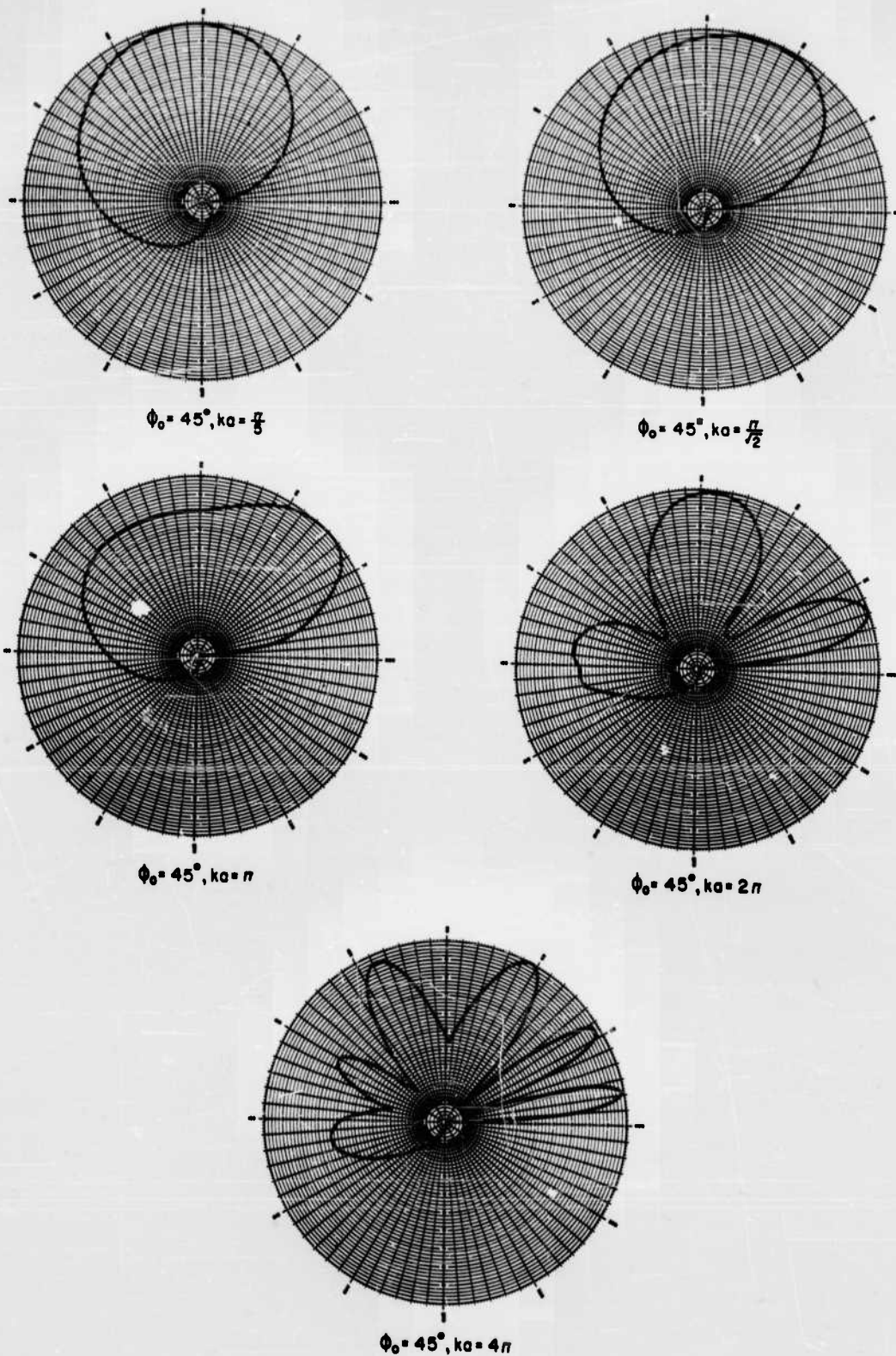


FIG. 2D
RADIATION PATTERN OF A LONGITUDINAL DIPOLE
PLACED IN FRONT OF A HALF-PLANE SHEET

D-591-TR45-491

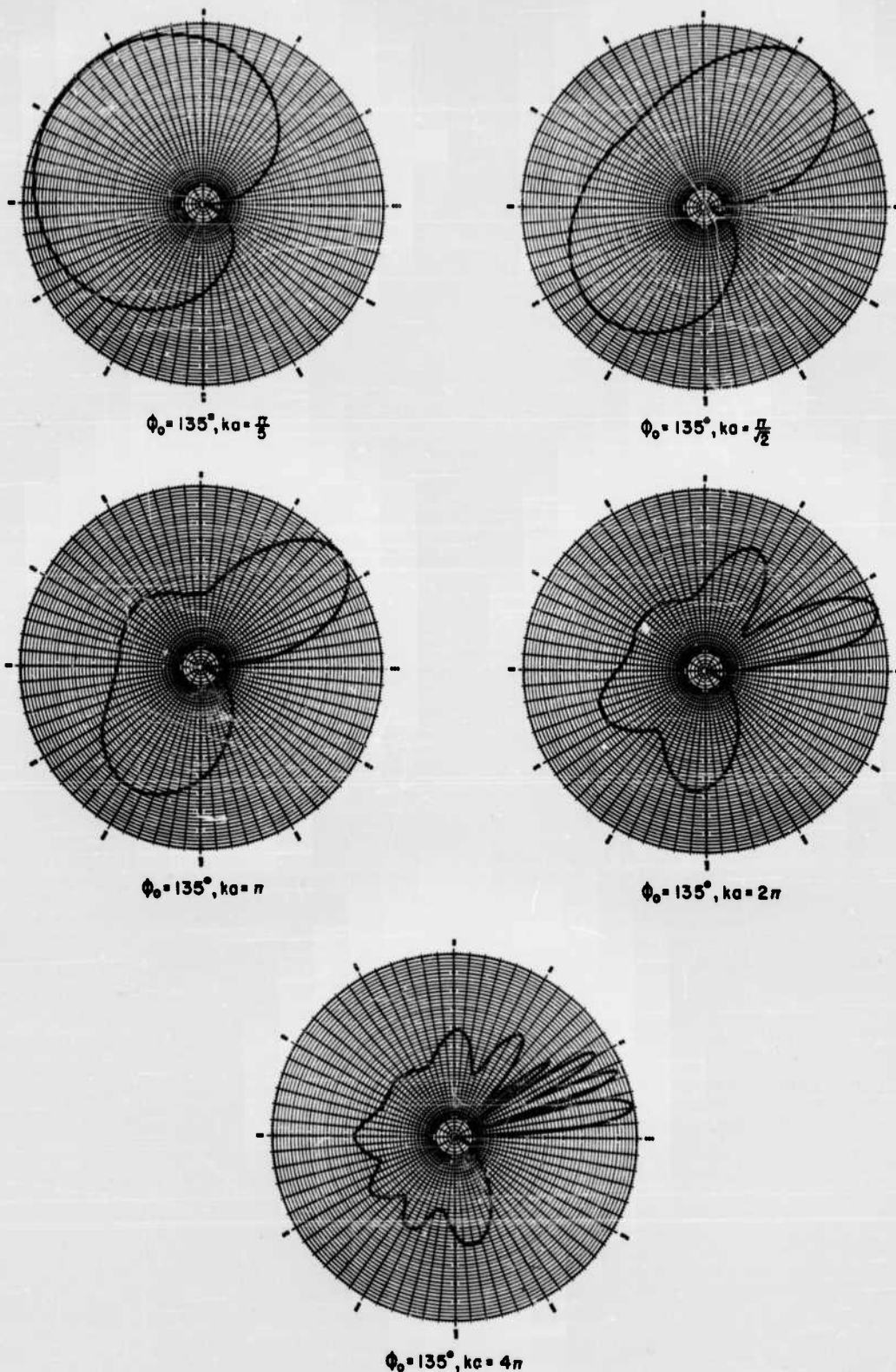
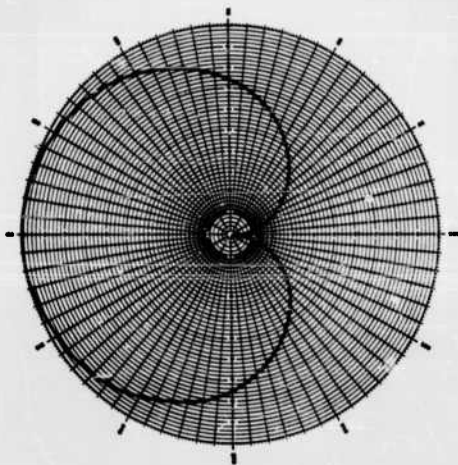


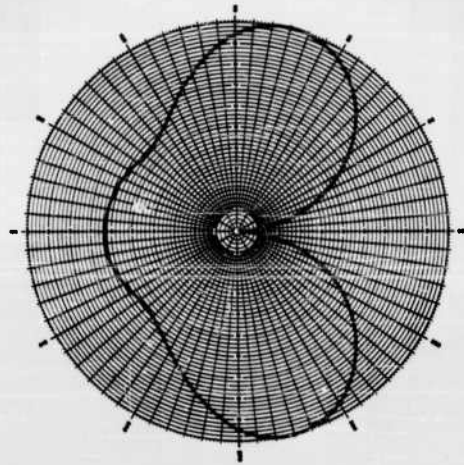
FIG. 2E

RADIATION PATTERN OF A LONGITUDINAL DIPOLE
PLACED IN FRONT OF A HALF-PLANE SHEET

D-591-TR46-492

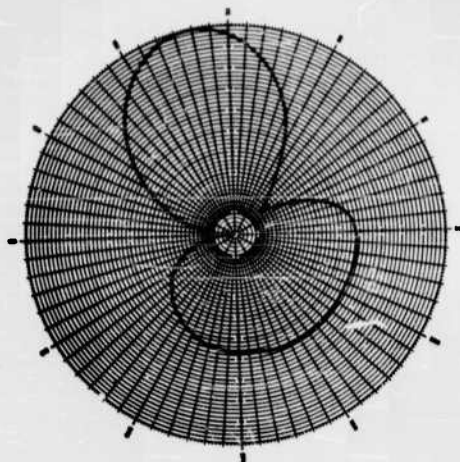


$$\phi_0 = 180^\circ, ka = \frac{\pi}{5}$$

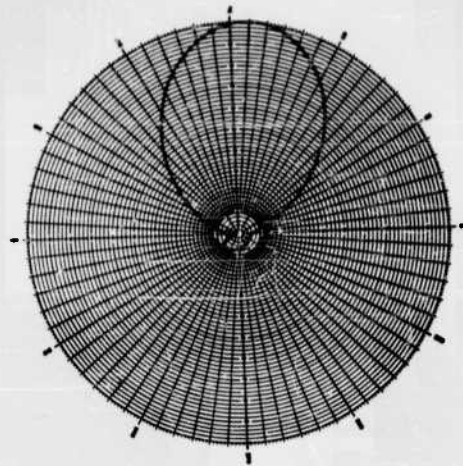


$$\phi_0 = 180^\circ, ka = \pi$$

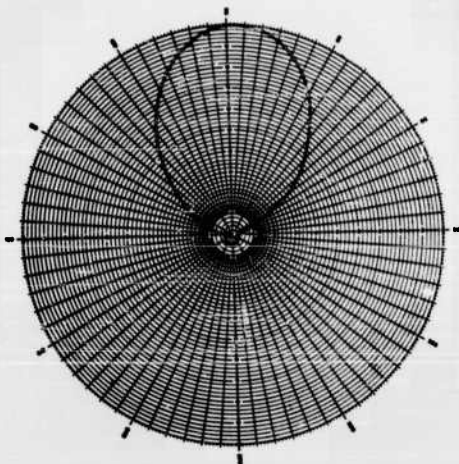
FIG. 2F
RADIATION PATTERN OF A LONGITUDINAL DIPOLE
PLACED IN FRONT OF A HALF-PLANE SHEET
D-591-TR45-493



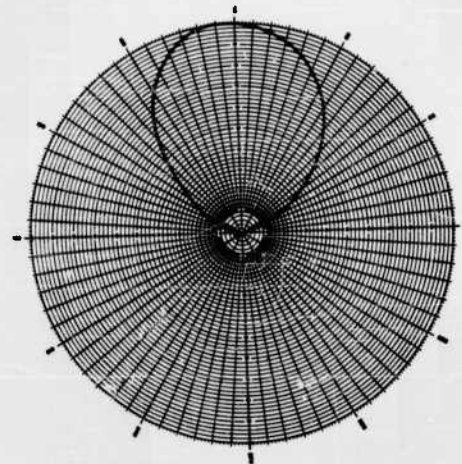
$$\phi_0 = 5^\circ, ka = \frac{\pi}{5}$$



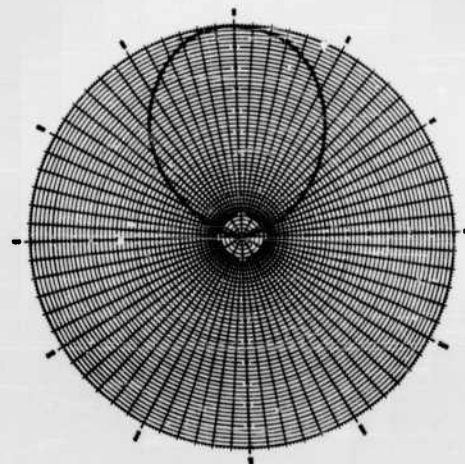
$$\phi_0 = 5^\circ, ka = \frac{\pi}{\sqrt{2}}$$



$$\phi_0 = 5^\circ, ka = \pi$$



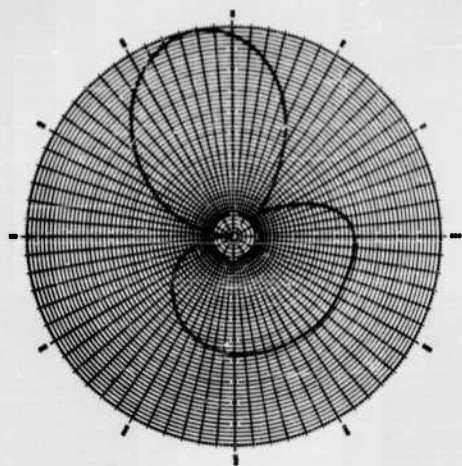
$$\phi_0 = 5^\circ, ka = 2\pi$$



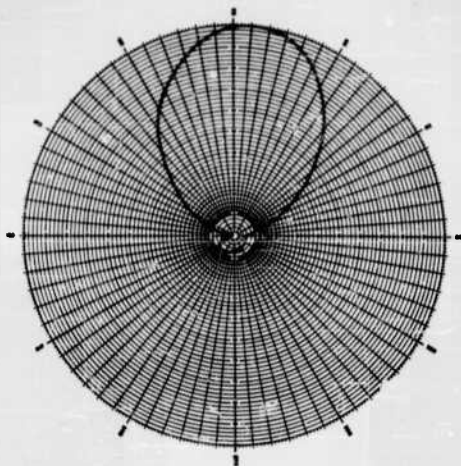
$$\phi_0 = 5^\circ, ka = 4\pi$$

FIG. 3A
RADIATION PATTERN OF A HORIZONTAL DIPOLE
PLACED IN FRONT OF A HALF-PLANE SHEET

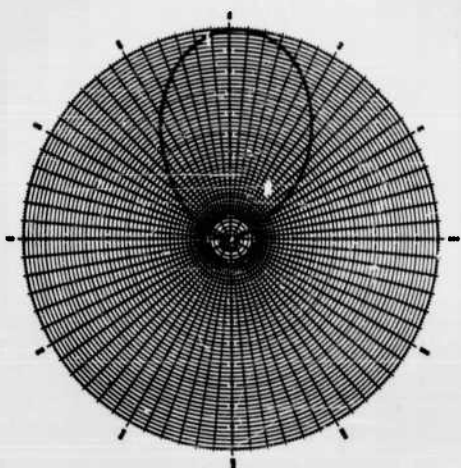
D-591-TR45-494



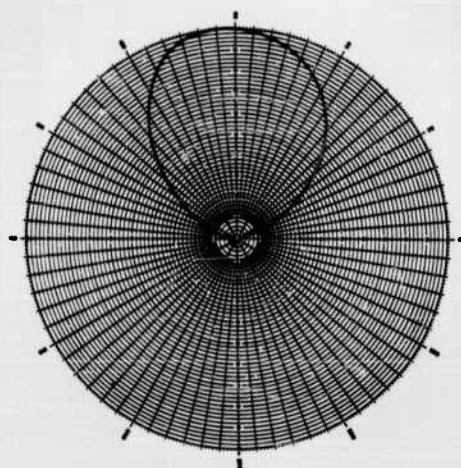
$$\phi_0 = 10^\circ, ka = \frac{\pi}{5}$$



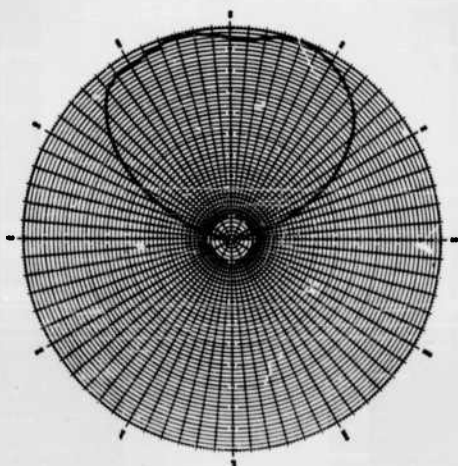
$$\phi_0 = 10^\circ, ka = \frac{\pi}{2}$$



$$\phi_0 = 10^\circ, ka = \pi$$



$$\phi_0 = 10^\circ, ka = 2\pi$$

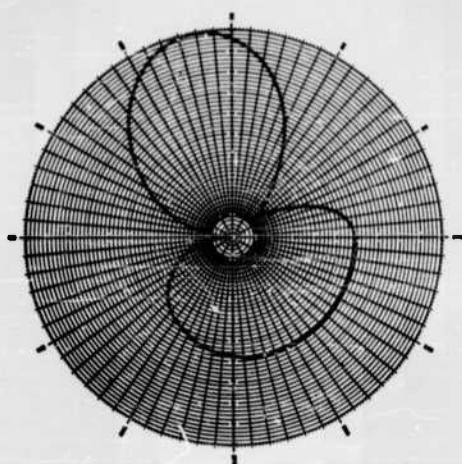


$$\phi_0 = 10^\circ, ka = 4\pi$$

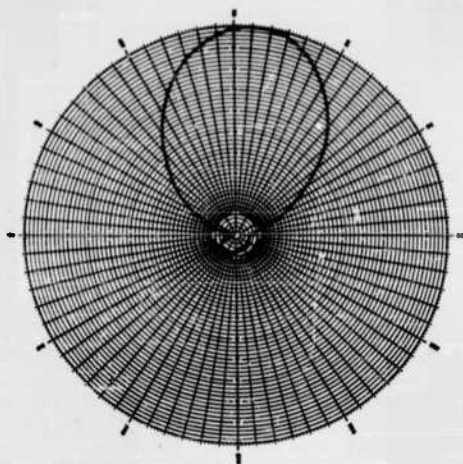
FIG. 3B

RADIATION PATTERN OF A HORIZONTAL DIPOLE
PLACED IN FRONT OF A HALF-PLANE SHEET

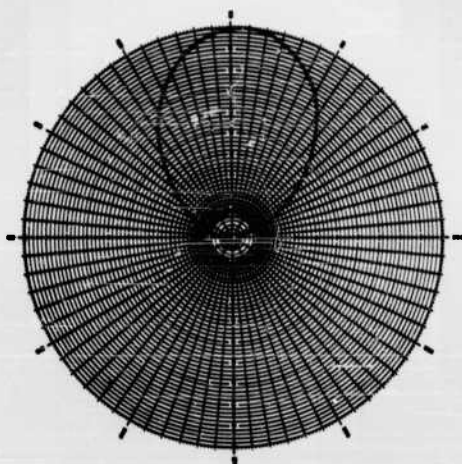
D-591-TR45-495



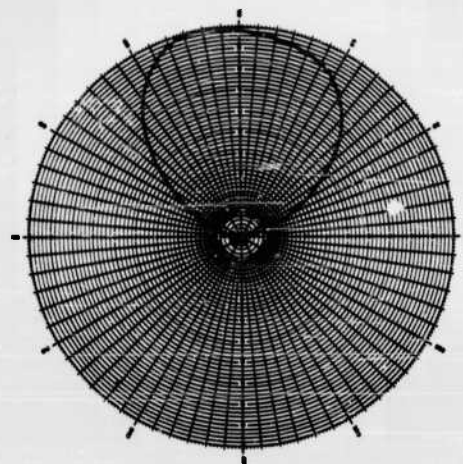
$$\phi_0 = 15^\circ, ka = \frac{\pi}{8}$$



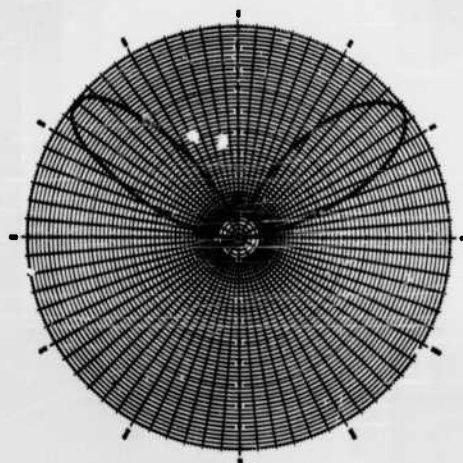
$$\phi_0 = 15^\circ, ka = \frac{\pi}{\sqrt{2}}$$



$$\phi_0 = 15^\circ, ka = \pi$$

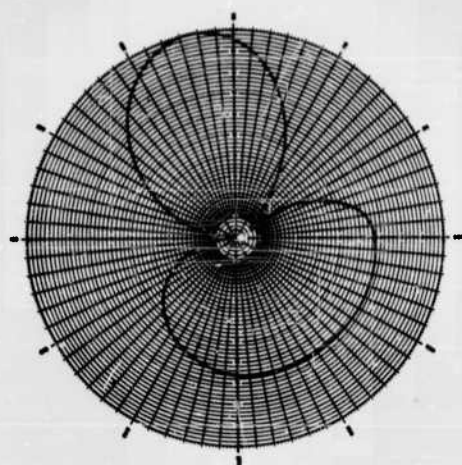


$$\phi_0 = 15^\circ, ka = 2\pi$$

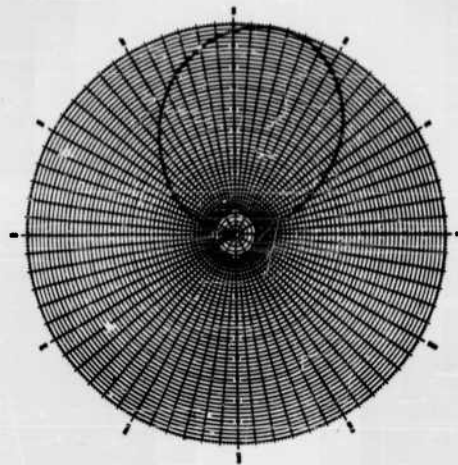


$$\phi_0 = 15^\circ, ka = 4\pi$$

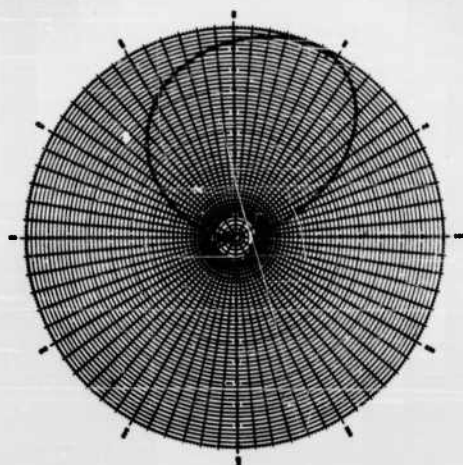
FIG. 3C
RADIATION PATTERN OF A HORIZONTAL DIPOLE
PLACED IN FRONT OF A HALF-PLANE SHEET
D-591-TR45-496



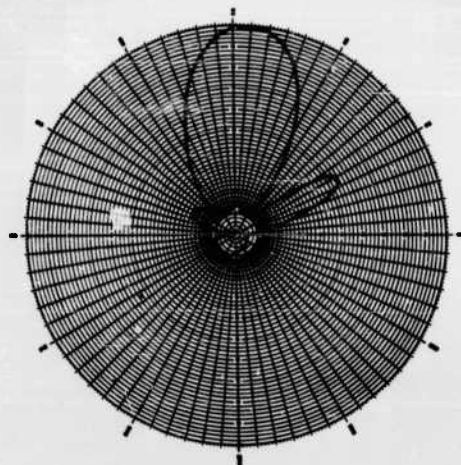
$$\phi_0 = 45^\circ, ka = \frac{\pi}{5}$$



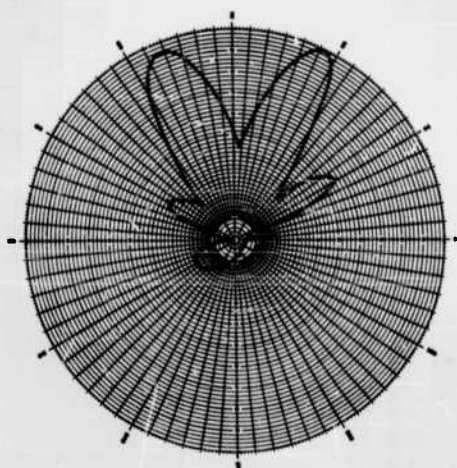
$$\phi_0 = 45^\circ, ka = \frac{\pi}{\sqrt{2}}$$



$$\phi_0 = 45^\circ, ka = \pi$$



$$\phi_0 = 45^\circ, ka = 2\pi$$

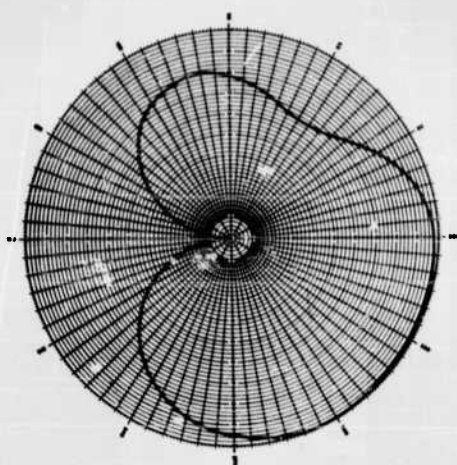


$$\phi_0 = 45^\circ, ka = 4\pi$$

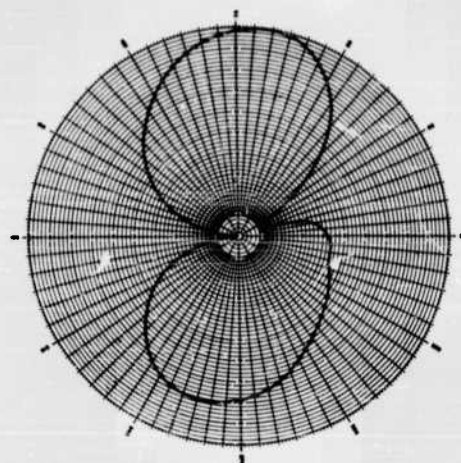
FIG. 3D

RADIATION PATTERN OF A HORIZONTAL DIPOLE
PLACED IN FRONT OF A HALF-PLANE SHEET

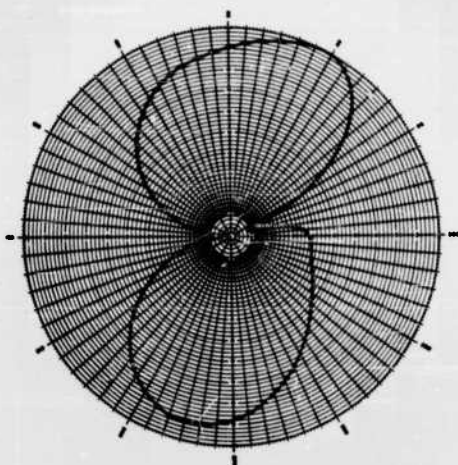
D-591-TR45-497



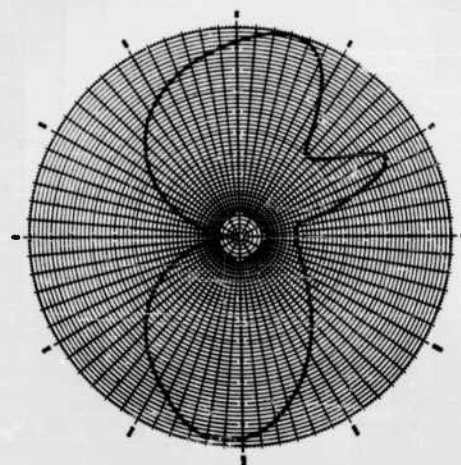
$$\phi_0 = 135^\circ, ka = \frac{\pi}{5}$$



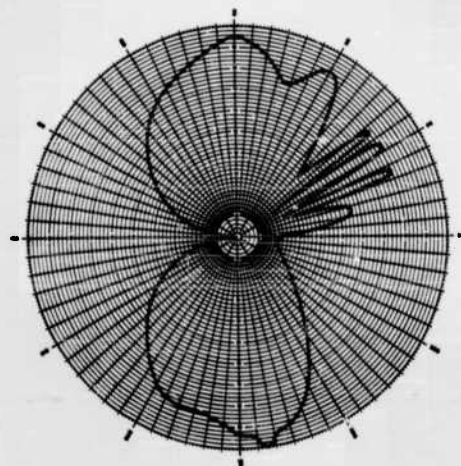
$$\phi_0 = 135^\circ, ka = \frac{\pi}{\sqrt{2}}$$



$$\phi_0 = 135^\circ, ka = \pi$$



$$\phi_0 = 135^\circ, ka = 2\pi$$

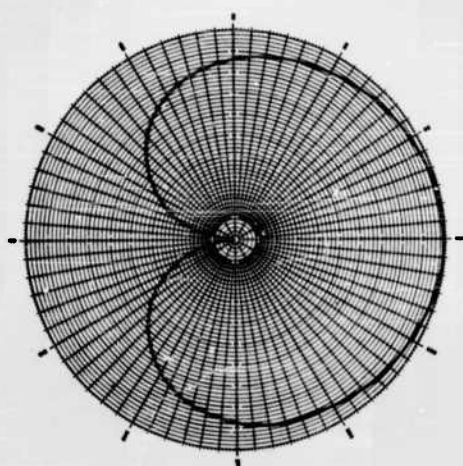


$$\phi_0 = 135^\circ, ka = 4\pi$$

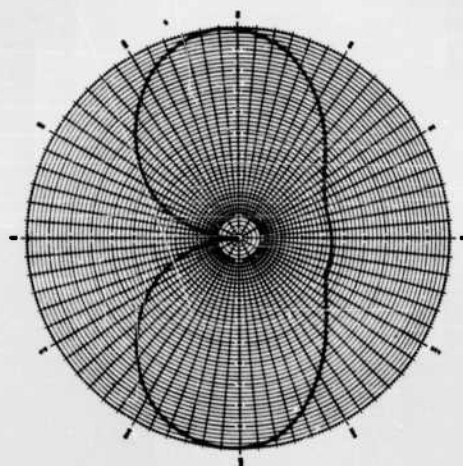
FIG. 3E

RADIATION PATTERN OF A HORIZONTAL DIPOLE
PLACED IN FRONT OF A HALF-PLANE SHEET

D-591-TR4 -498



$$\phi_0 = 180^\circ, ka = \frac{\pi}{5}$$



$$\phi_0 = 180^\circ, ka = \pi$$

FIG. 3F

RADIATION PATTERN OF A HORIZONTAL DIPOLE
PLACED IN FRONT OF A HALF-PLANE SHEET

C-591-TR45-499

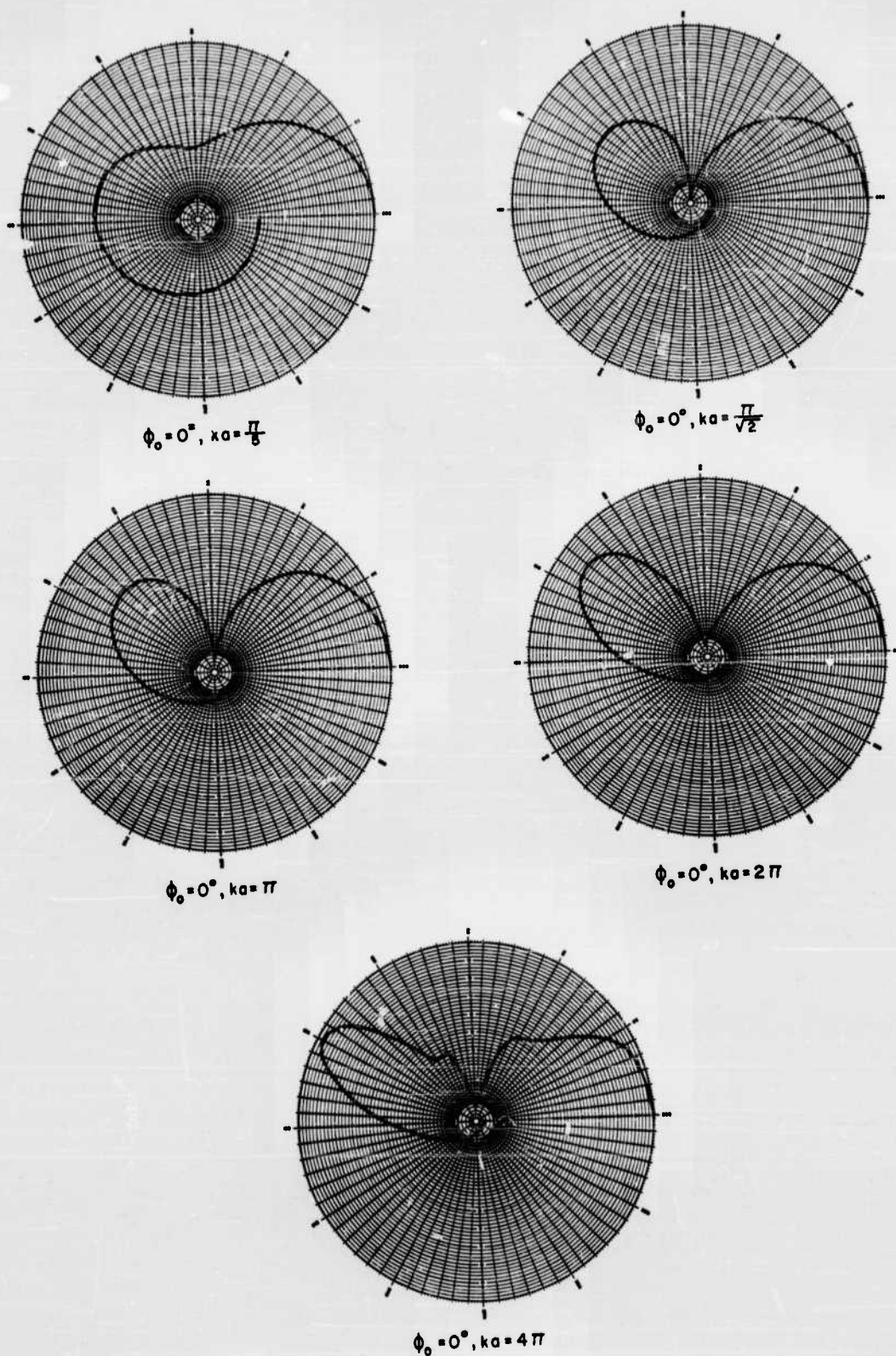


FIG. 4A

RADIATION PATTERN OF A VERTICAL DIPOLE
PLACED IN FRONT OF A HALF-PLANE SHEET

D-591-TR45-500

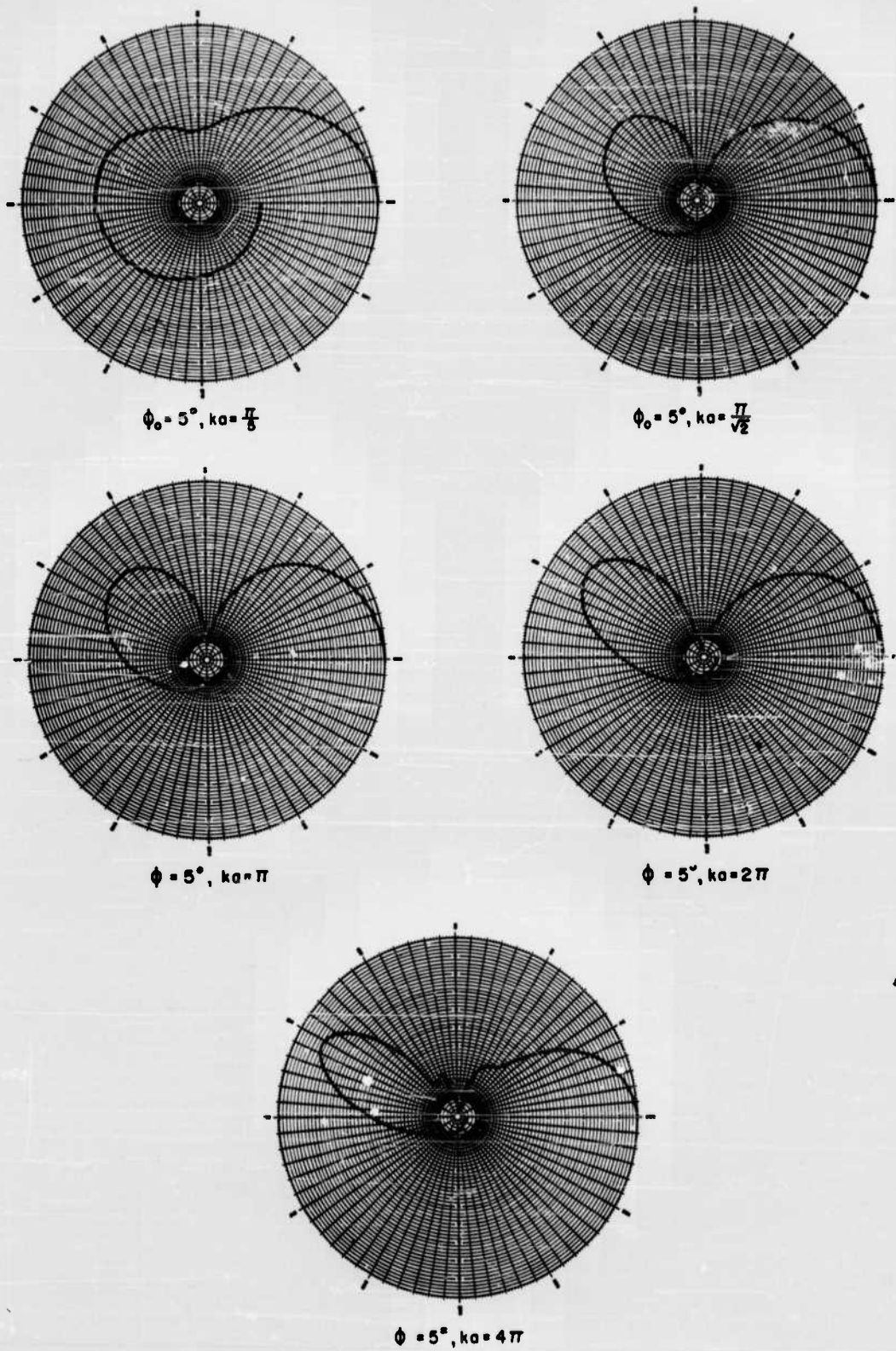
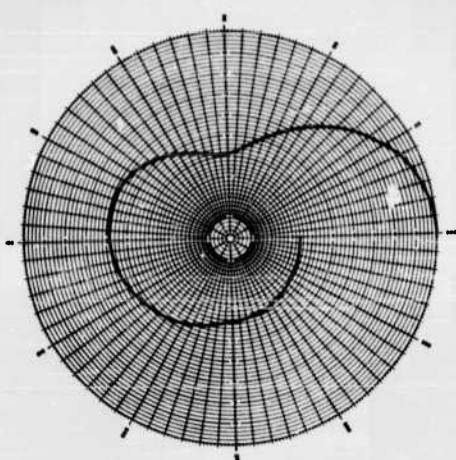


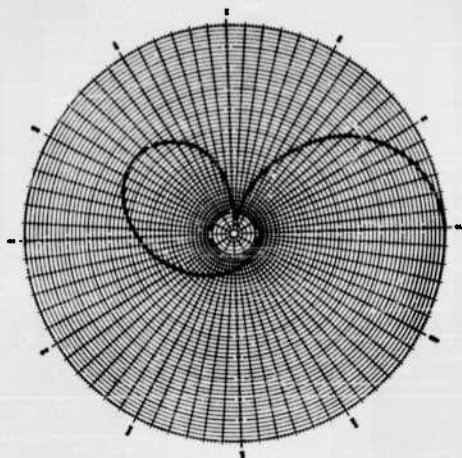
FIG. 4B

RADIATION PATTERN OF A VERTICAL DIPOLE
PLACED IN FRONT OF A HALF-PLANE SHEET

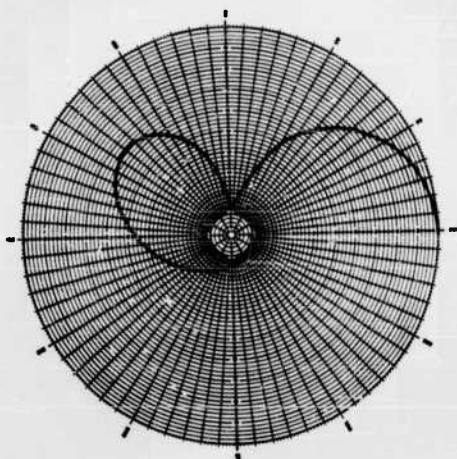
D-591-TR45-501



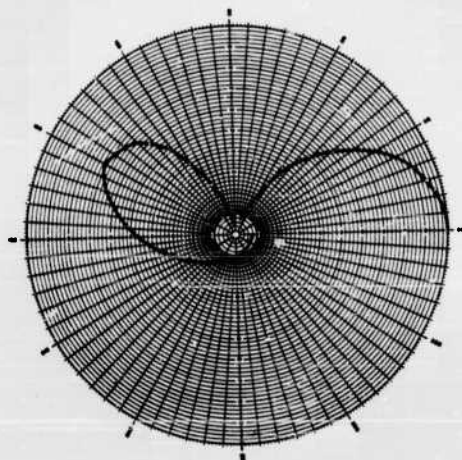
$$\phi_0 = 10^\circ, ka = \frac{\pi}{5}$$



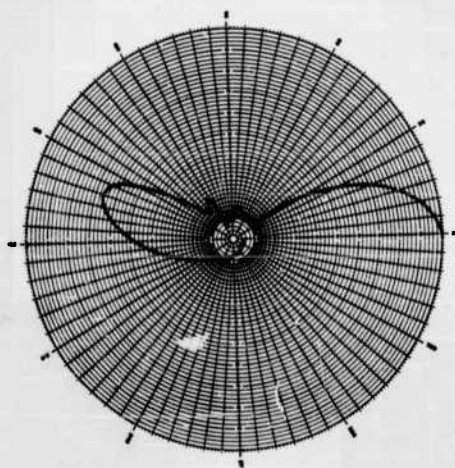
$$\phi_0 = 10^\circ, ka = \frac{\pi}{\sqrt{2}}$$



$$\phi_0 = 10^\circ, ka = \pi$$



$$\phi_0 = 10^\circ, ka = 2\pi$$



$$\phi_0 = 10^\circ, ka = 4\pi$$

FIG. 4C

RADIATION PATTERN OF A VERTICAL DIPOLE
PLACED IN FRONT OF A HALF-PLANE SHEET

D-591-TR45-502

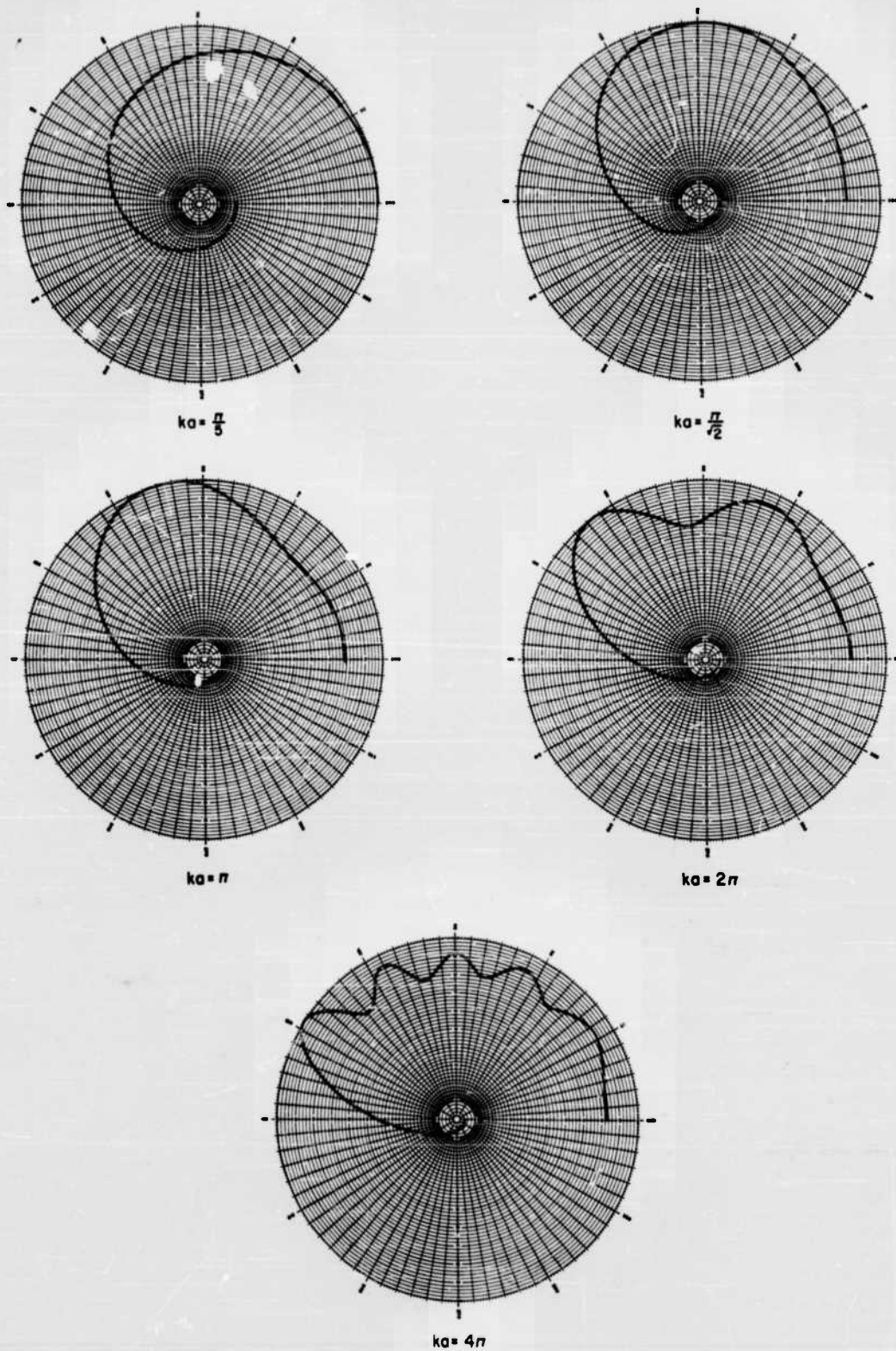


FIG. 5
RADIATION PATTERN OF A ONE-SIDED LONGITUDINAL SLOT
D-591-TR45-503

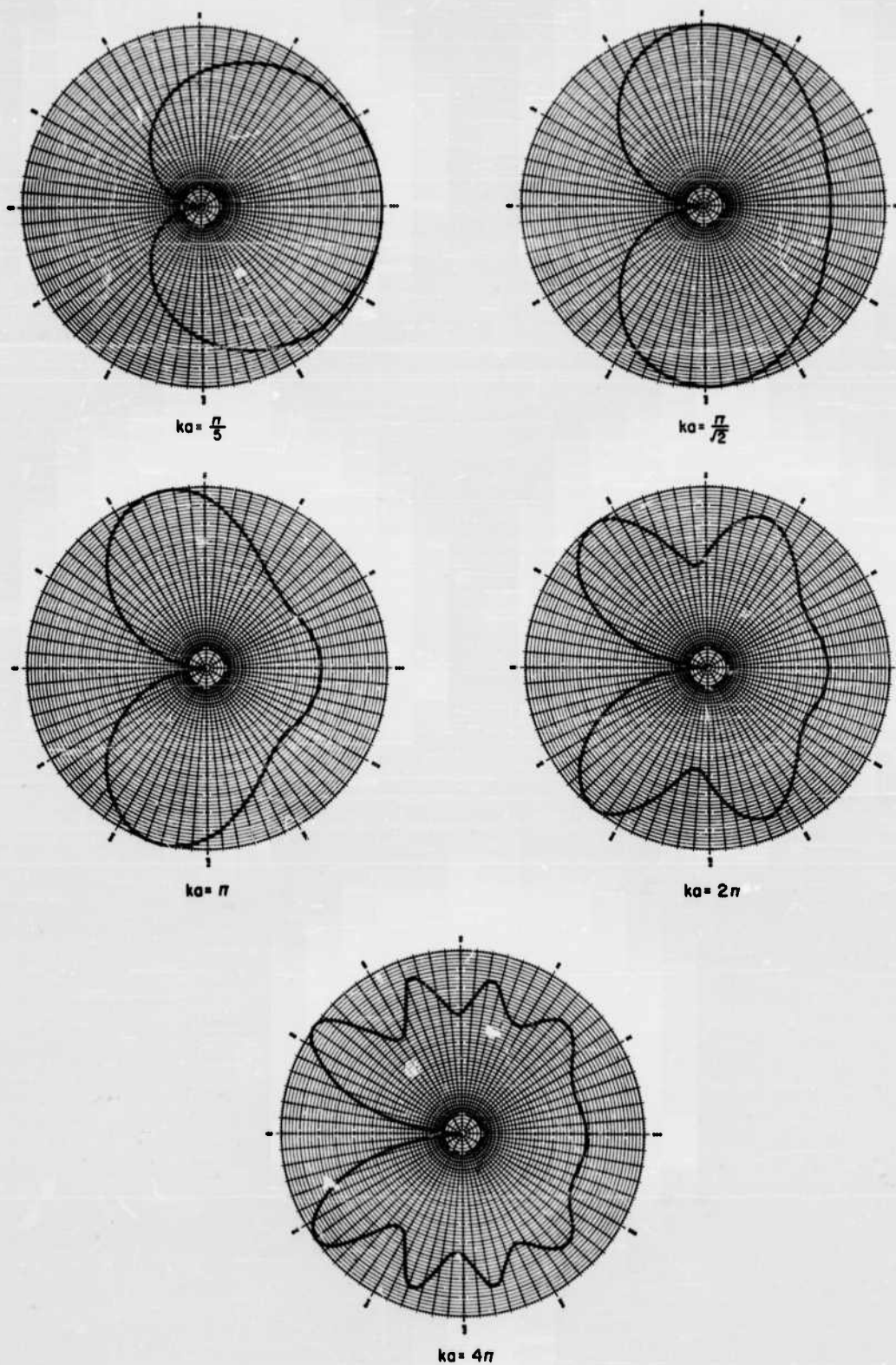


FIG. 6
 RADIATION PATTERN OF A TWO-SIDED LONGITUDINAL SLOT
 D-591-TR45-504

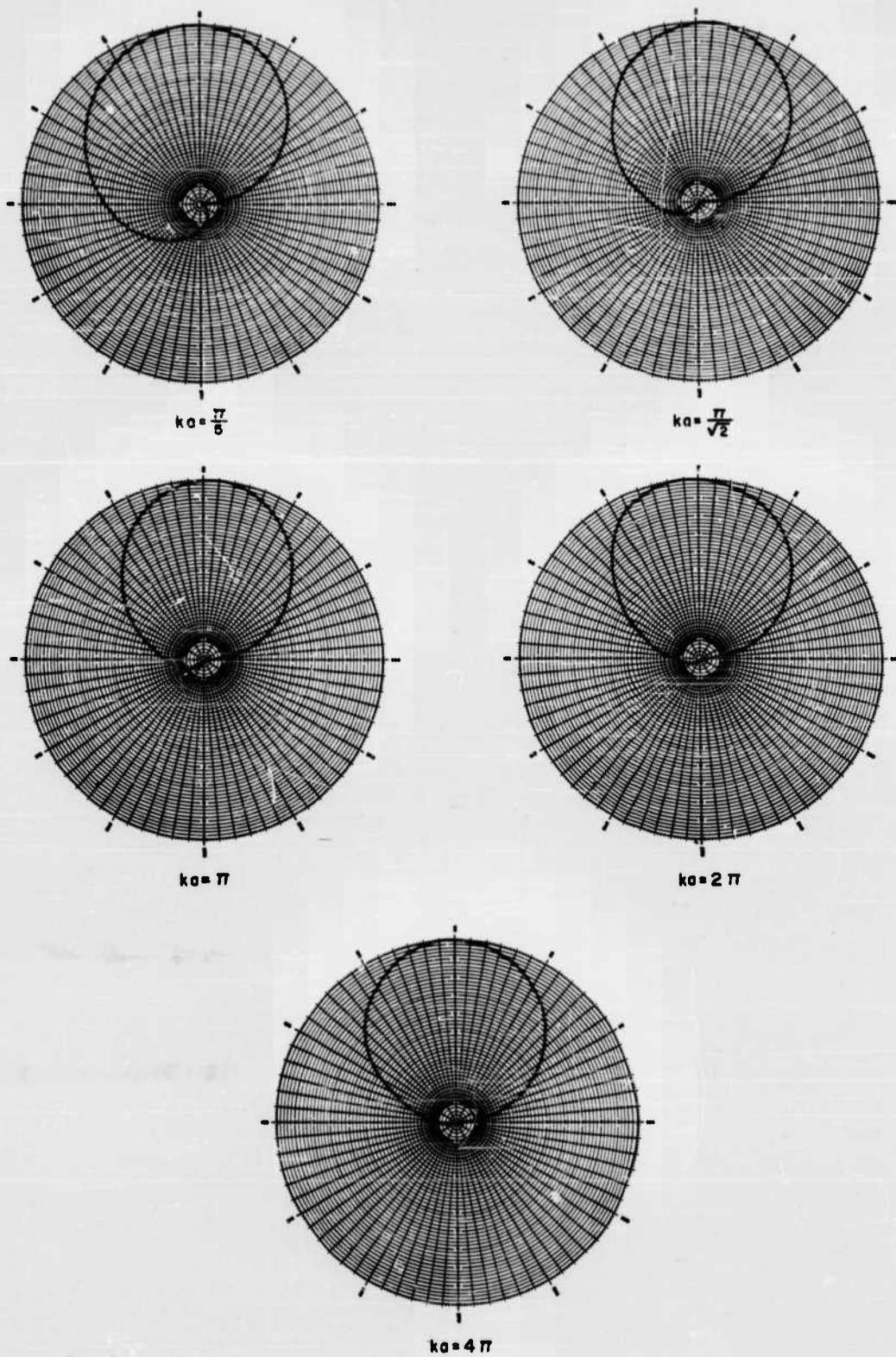


FIG. 7

RADIATION PATTERN OF A SMALL ONE-SIDED HORIZONTAL APERTURE

D-591-TR45-505

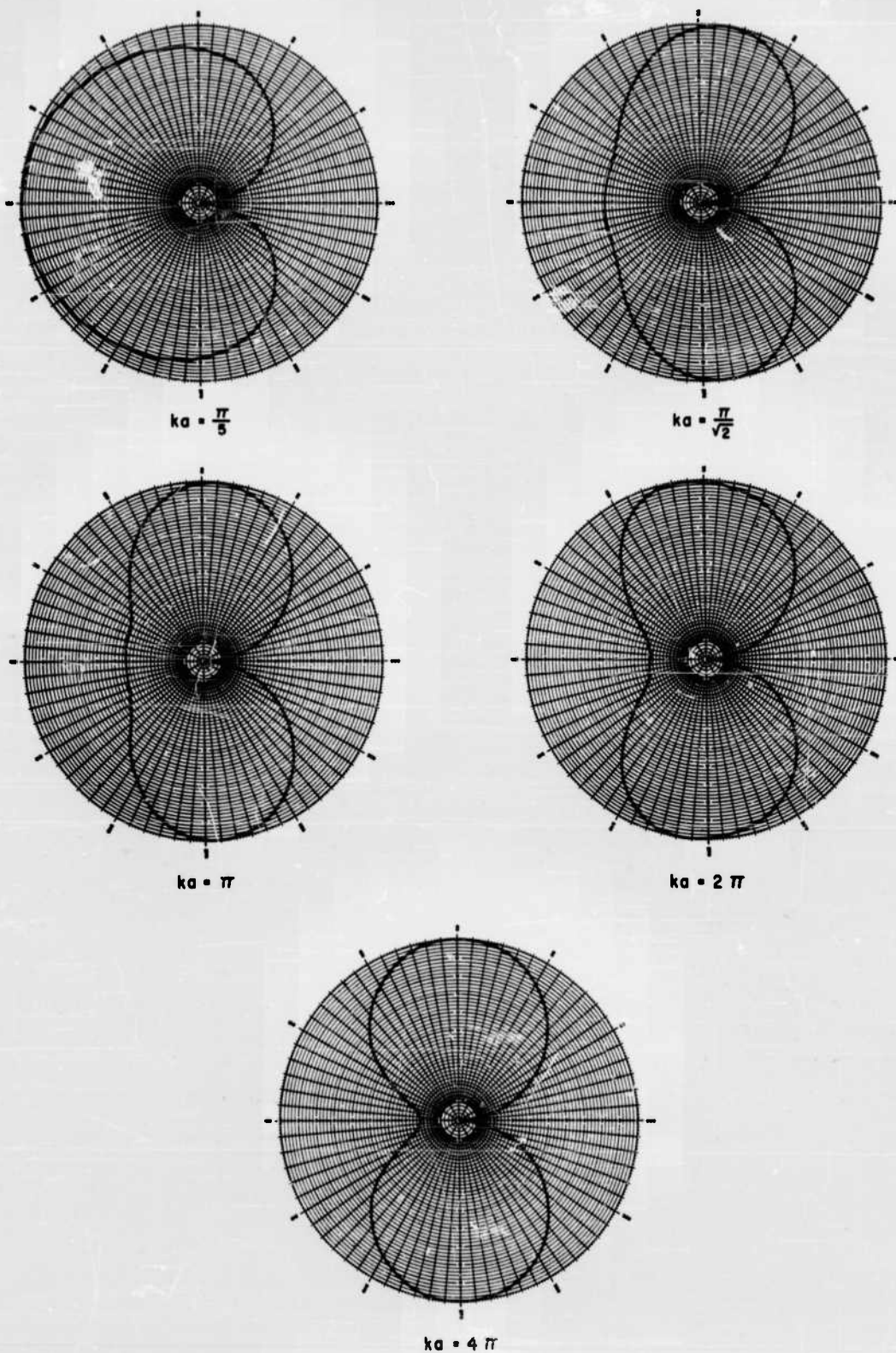


FIG. 2

RADIATION PATTERN OF A SMALL TWO-SIDED HORIZONTAL APERTURE

D-591-TR45-506

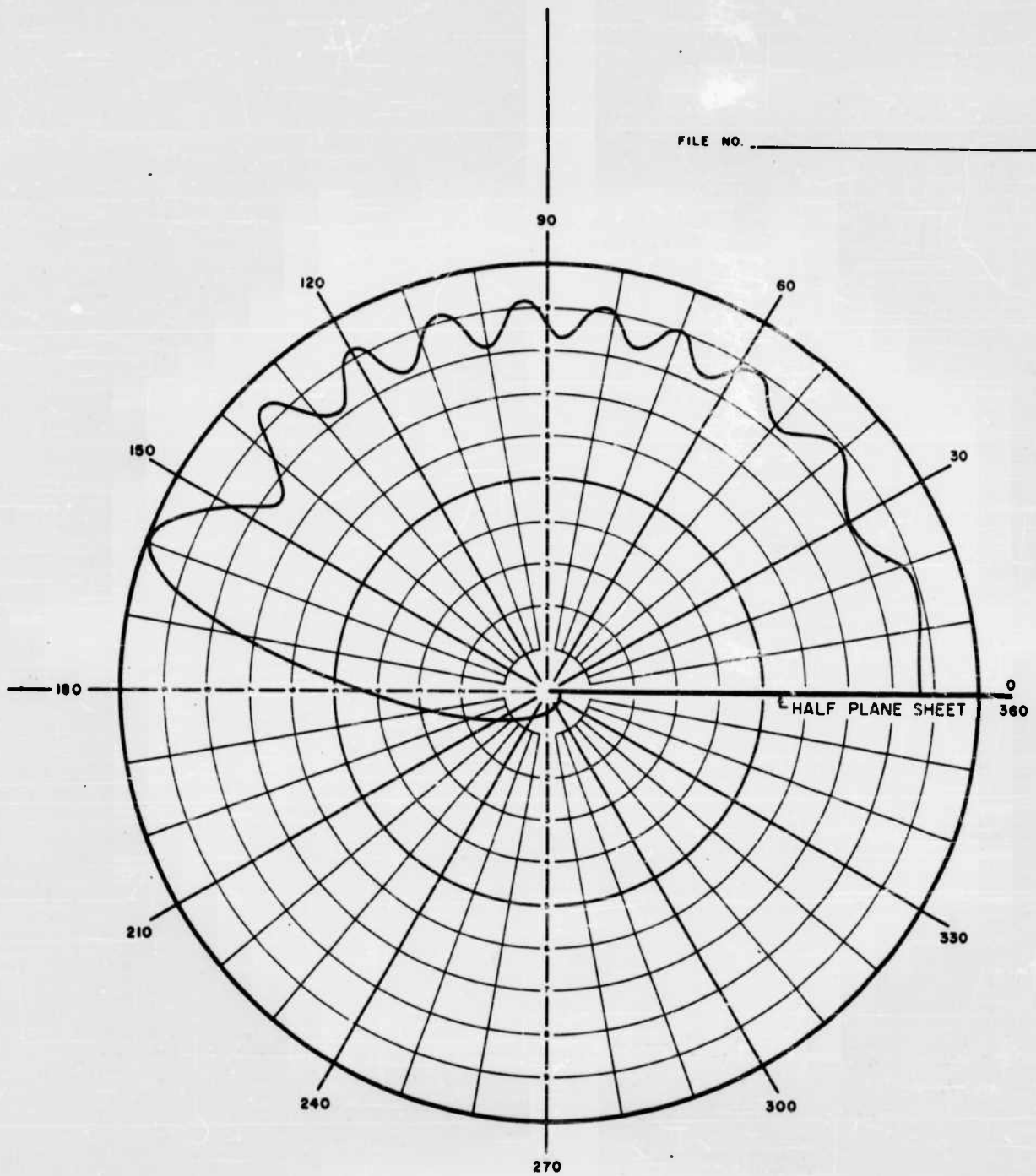


FIG. 9
RADIATION PATTERN OF A LONGITUDINAL
SLOT PLACED AT $ka = 30$

A-591-TR48-507



FIG. 10

ROOTS OF THE EQUATION $\frac{0.5+C(x)}{0.5+S(x)} = -\tan x$

A-591-TR45-508

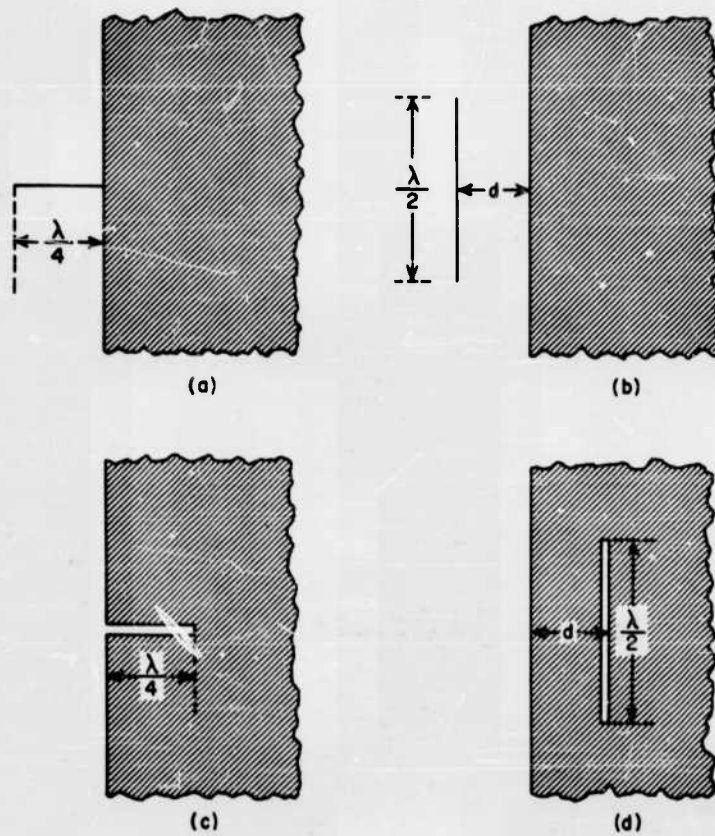


FIG. II
 DIPOLES AND SLOTS WITH A HALF-PLANE SHEET
 A-591-TR45-509

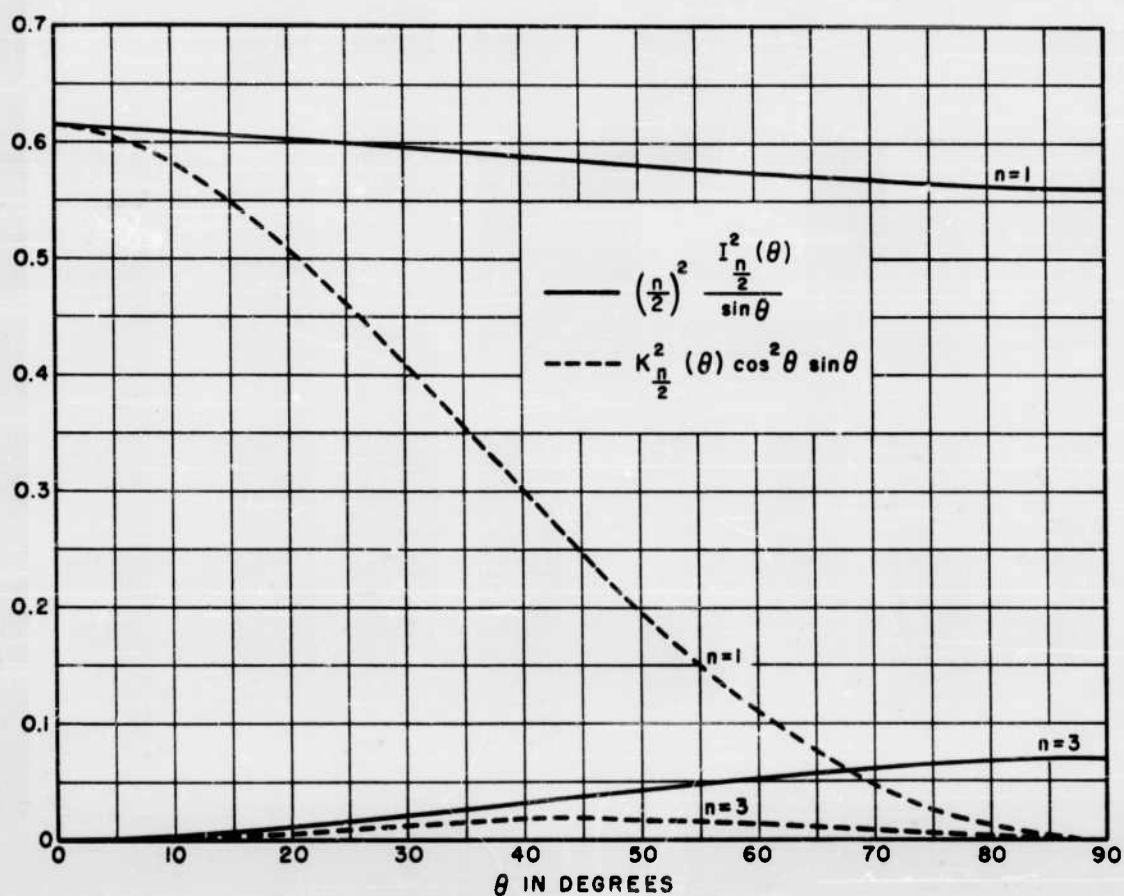


FIG. 12

THE FUNCTIONS $\left(\frac{n}{2}\right)^2 \frac{I_{\frac{n}{2}}^2(\theta)}{\sin \theta}$ AND $K_{\frac{n}{2}}^2(\theta) \cos^2 \theta \sin \theta$

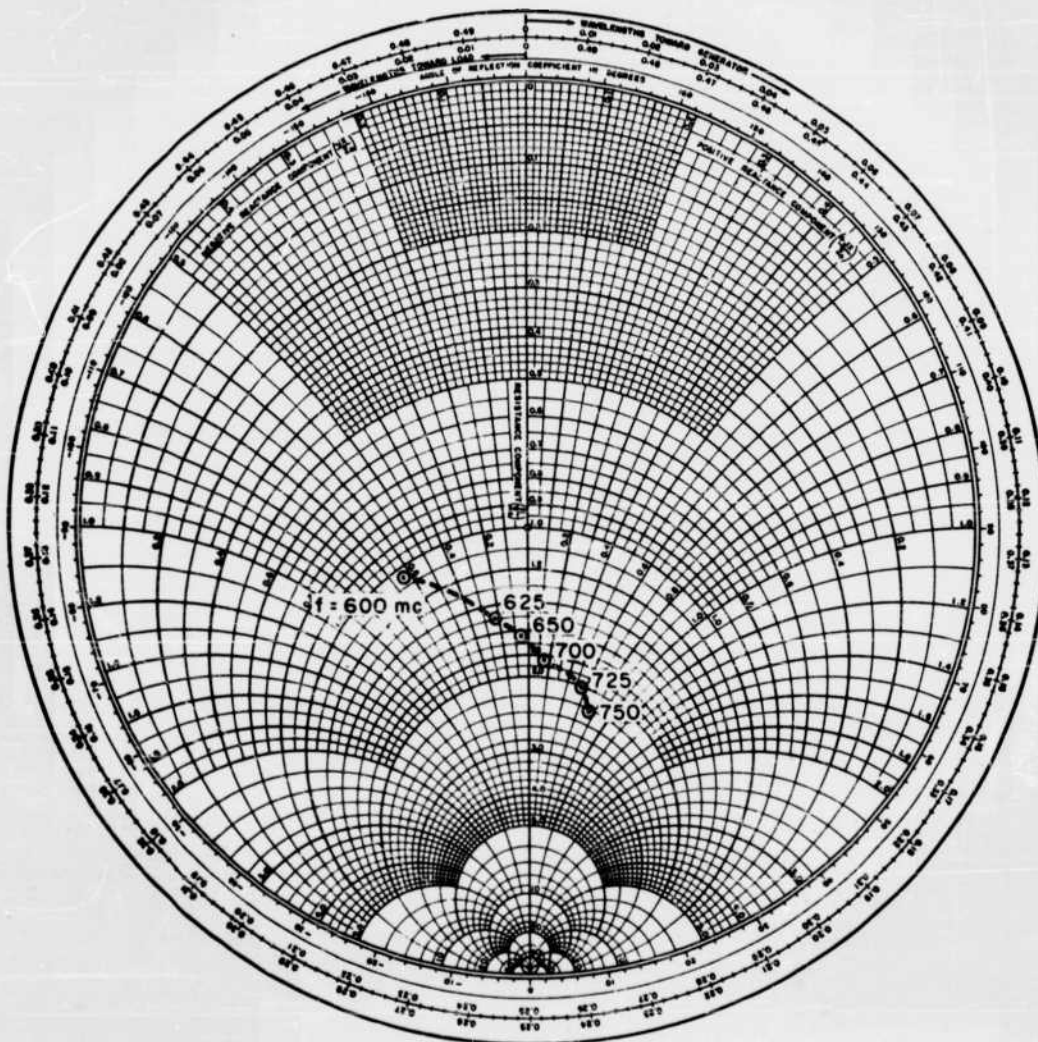
A-591-TR45-510

RADIO SYSTEMS LABORATORY

PROJECT _____

DATE _____

FILE NO. _____



IMPEDANCE DATA _____ Z_c 50 OHMS

ANTENNA $4\frac{1}{2}$ " STUB ON THE EDGE OF A 6'x8'4" ALUMINUM

SHEET OF THICKNESS $\frac{1}{8}$ "

FIG. 13

INPUT IMPEDANCE OF A STUB PLACED
AT THE EDGE OF A HALF-PLANE SHEET

A-591-TR45-511

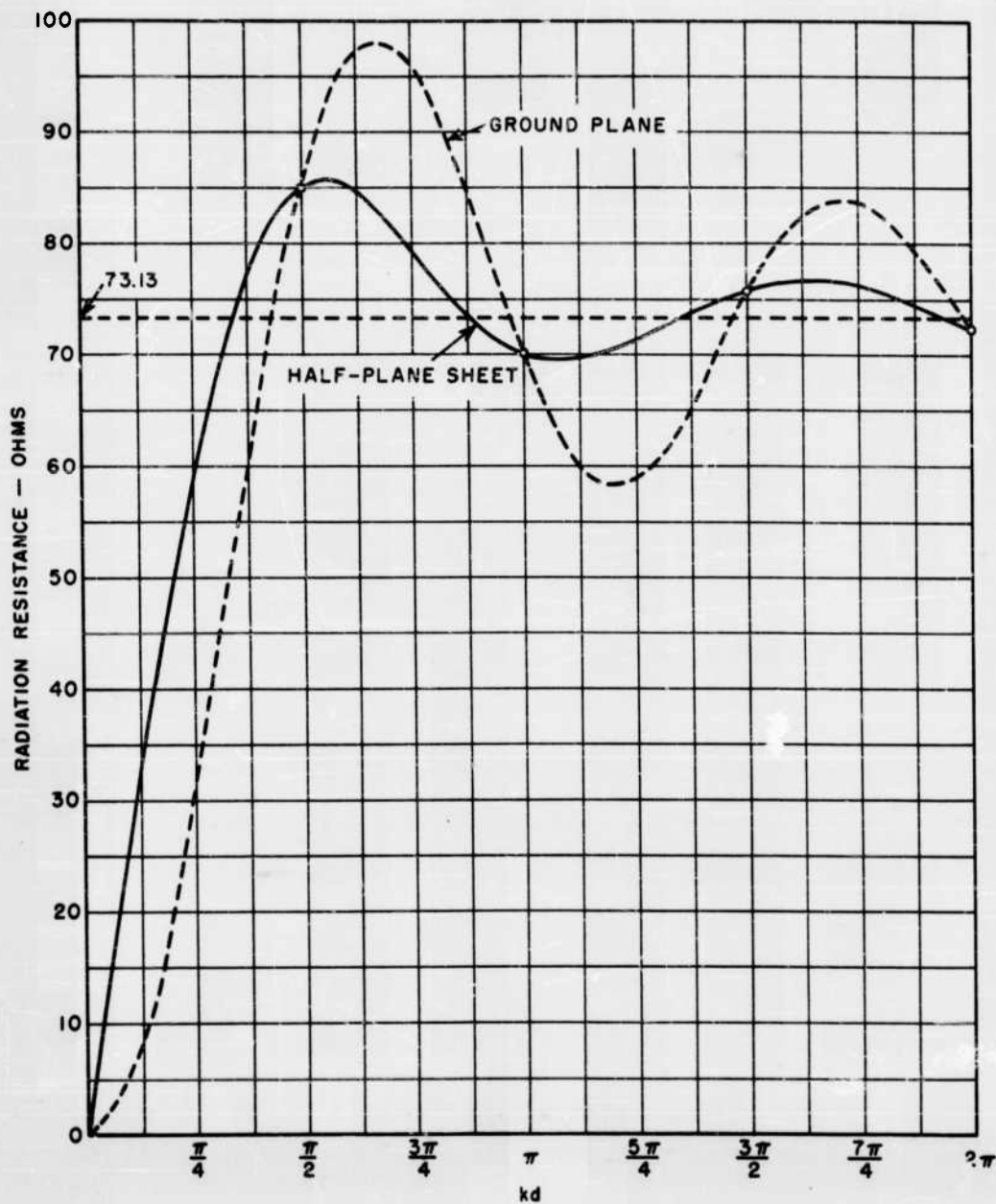


FIG. 14

RADIATION RESISTANCE OF A HALF-WAVE DIPOLE PLACED IN FRONT
OF A HALF-PLANE SHEET, AND IN FRONT OF A GROUND PLANE.

A-591-TR45-512

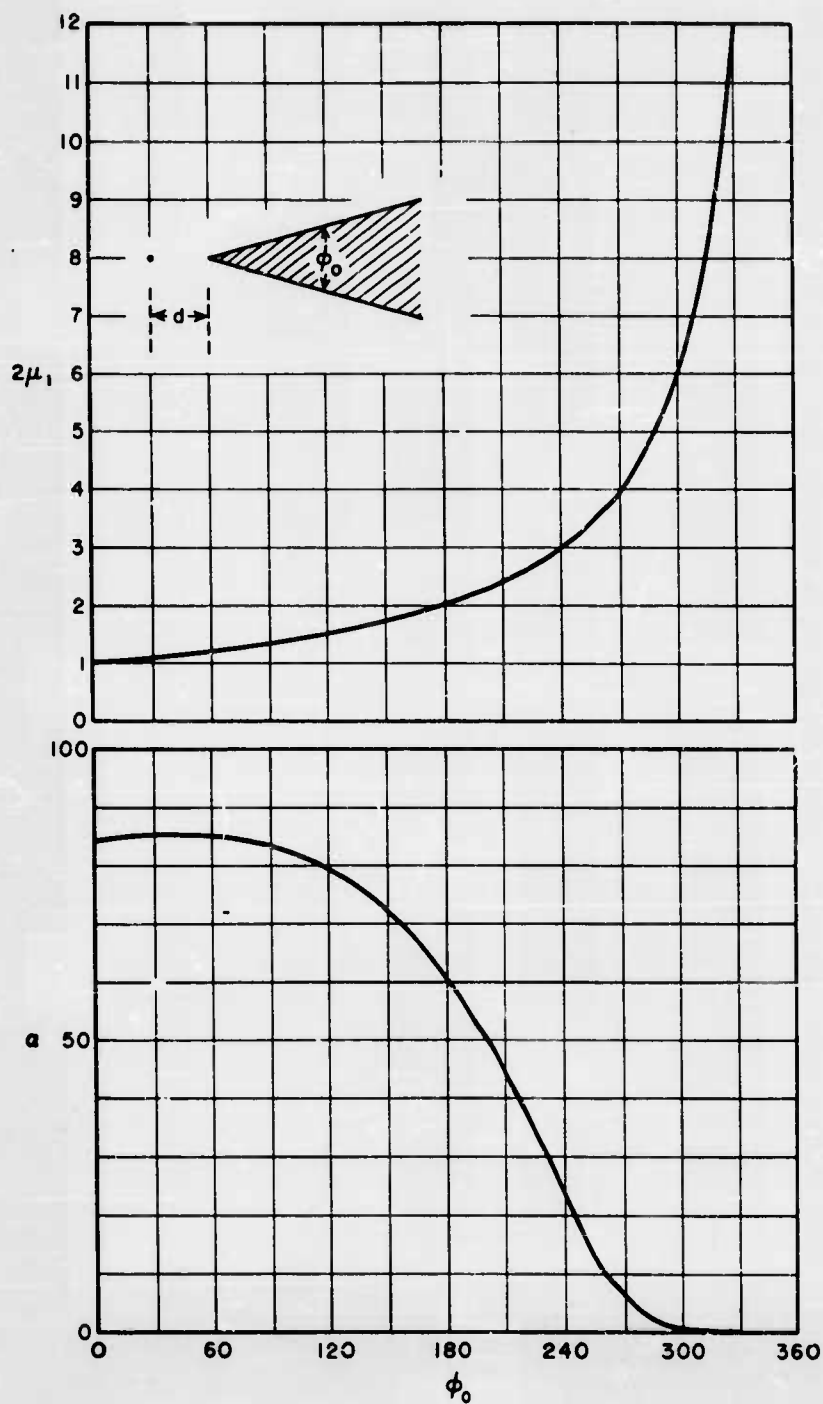


FIG. 15
RADIATION RESISTANCE OF A HALF-WAVE DIPOLE
PLACED NEAR A WEDGE, $R_d = a(kd)^2 \mu_1$ IN OHMS

A-591-TR45-513

TECHNICAL REPORTS IN THIS SERIES

Reports Issued on Contract AF 19(122) - 78

1. "Electric Dipoles in the Presence of Elliptic and Circular Cylinders" by W. S. Lucke, September 1949.
2. "Assymmetrically-Fed Antennas," by C. T. Tai, November 1949.
3. "Double-Fed and Coupled-Antennas," by C. T. Tai, February 1949.
4. "Equivalent Radii of Thin Cylindrical Antennas with Arbitrary Cross Sections," by Carson Flammer, March 1950.
5. "Use of Complementary Slots in Aircraft Antenna Impedance Measurements" by J. T. Bolljahn, February 1950.
6. "Wing-Cap and Tail-Cap Aircraft Antennas," by J. V. N. Granger, March 1950.
7. "Investigation of Current Distribution on Asymmetrically-Fed Antennas by Means of Complementary Slots," by R. M. Hatch, Jr., February 1950.
8. "Electromagnetic Resonance Phenomena in Aircraft Structures," by A. S. Dunbar, May 1950.
9. "The Effect of a Grounded Slab on the Radiation from a Line Source," by C. T. Tai, June 1950.
10. "A Method for the Calculation of Progressive-Phase Antennas for Shaped Beams," by A. S. Dunbar, June 1950.
11. "Admittance of an Open Ended Coaxial Line in an Infinite Grounded Plane," by W. S. Lucke, June 1950.
12. "A Variational Solution to the Problem of Cylindrical Antennas," by C. T. Tai, August 1950.
13. "Uniform Progressive Phase Antennas Having Asymmetrical Amplitude Distributions," by A. S. Dunbar, September 1950.
14. "Small Dipole-Type Antennas," by J. T. Bolljahn, September 1950.
15. "Tables of Modified Cosine Integrals," January 1951.
16. "Prolate Spheroidal Wave Functions," by Carson Flammer, February 1951.
17. "An Antenna Evaluation Method," by W. S. Lucke, April 1951.
18. "Radar Response from Thin Wires," by C. T. Tai, March 1951.
19. "The Measurement of Low-Frequency Aircraft Antenna Properties Using Electrostatic Methods," by J. T. Bolljahn, September 1951.

20. (Dropped)
21. "A Method for the Calculation of Progressive-Phase Antennas for Shaped Beams," Part II, by A. S. Dunbar, May 1951.
22. "The Prolate Spheroidal Monopole Antenna," by Carson Flammer [pending, Issued on contract AF 19(604) - 266].
23. "Variational Solution for the Problem of the Asymmetric Dipole," by I. Reese, August 1951.
24. "Quasi-Static Solution for Diffraction of a Plane Electromagnetic Wave by a Small Oblate Spheroid," by C. T. Tai, September 1952 [issued on contract AF 19(604) - 266].
25. "Transmission Through a Rectangular Aperture in an Infinite Screen," by W. S. Lucke, September 1951.

Reports Issued on Contract AF 19(604) - 266

26. "Improvements in Instrumentation for the Investigation of Aircraft Antenna Radiation Patterns by Means of Scale Models," by R. M. Hatch, Jr., August 1952.
27. "The Vector Wave Solution of the Diffraction of Electromagnetic Waves by Circular Disks and Apertures," by Carson Flammer, September 1952.
28. "An Investigation of the Distribution of Current on Collinear Parasitic Antenna Elements," by R. M. Hatch, Jr., August 1952.
29. "On the Theory of Diffraction of Electromagnetic Waves by a Sphere," by C. T. Tai, October 1952.
30. "High-Frequency Airborne Direction Finding," by P. S. Carter, Jr., December 1952.
31. "An Electrolytic Tank Method for Low-Frequency Loop Antennas Studies," by R. F. Reese, July 1953.
32. "Radiation from a Uniform Circular Loop Antenna in the Presence of a Sphere," by C. T. Tai, December 1952.
33. "A Computer for Use with Antenna Model Ranges," by C. E. Fisher, February 1953.
34. "Tail-Cap Antenna Radiation Pattern Studies," by J. H. Bryan, January, 1953.
35. "Methods of Improving Tail Cap Antenna Patterns," by A. R. Ellis (pending)
36. "Mutual Admittance of Slots in Cylinder," by W. S. Lucke, February, 1953.

37. "Radio Interference from Corona Discharges," by R. L. Tanner, April, 1953.
38. "Effects of Airframe Configuration on Low-Frequency Antenna Characteristics," by C. M. Hoblitzell, April, 1953.
39. "Reference Antenna for Use with Model Pattern Ranges," by A. R. Ellis (pending).
40. "Analysis of the Overstation Behavior of Airborne ADF Systems," by H. H. Ward, (pending).
41. "Some Electromagnetic Problems Involving a Sphere," by C. T. Tai, April, 1953.
42. "Radiation Pattern Measurements of Stub and Slot Antennas on Spheres and Cylinders," by J. Bain, April, 1953.
43. "Current Distribution on Wing-Cap and Tail-Cap Antennas," by Irene C. Carswell, May 1954.
44. "A Study of Radiating Structures for Perpendicularly-Polarized Flush Radar Antennas," by Edward M. T. Jones and Seymour B. Cohn, July 1953.
45. "Radiation from Current Elements and Apertures in the Presence of a Perfectly Conducting Half-Plane Sheet," by C. T. Tai, July 1954